FINAL REPORT

ON

EVALUATION OF RELATIVE EFFECT OF NATURAL AND SYNTHETIC SEAWATERS IN CORROSION FATIGUE OF STEEL WELDED JOINTS

BY

C.C. Monahan
R.M. Hopkins

Faculty of Engineering and Applied Science
Memorial University of Newfoundland

WORK ON THIS PROJECT WAS CONDUCTED UNDER THE AUSPICES OF THE CANADA CENTRE FOR MINERAL & ENERGY TECHNOLOGY DEPARTMENT OF ENERGY, MINES & RESOURCES, CANADA

****

SSC File No. 04ST.23440-6-9202

DSS Contract Serial No. 23440-6-9202/01-ST

CANMET Project No. 708801

CANMET Scientific Authority: Dr. O. Vosikovsky

****

March/1988

MICROMEDIA

61 pp

THIS REPORT SHOULD BE CITED AS CONTRACT REPORT NO. 23440-6-9202/01-ST

ABSTRACT

Two solutions, ASTM substitute ocean water and natural seawater, are used more or less interchangeably to evaluate the fatigue crack growth properties of steels. There is evidence in the literature to suggest that the mechanism responsible for accelerated fatigue crack growth in cathodically protected steel (i.e. water reduction) can be significantly influenced by bulk solution chemistry. Experiments were designed to investigate the relative severity of these two solutions when used with cathodically protected steel samples. The investigation was conducted using three types of specimens: welded T-plates, compact type (CT) specimens and artificial crevices. Welded T-plates provided data on the initiation and propagation behavior of semi-elliptical cracks. CT specimens were tested to obtain crack growth rate versus crack tip stress intensity range data, since it is difficult to derive similar curves from welded T-plate data. The artificial crevice experiments were combined with polarographic and scanning electron microprobe (SEM) analyses to study the chemistry of calcareous deposits and their influence on water reduction kinetics.

The extent to which calcareous deposits affected the rate for water reduction within the artificial crevices depended on the bulk solution chemistry under which they formed. Magnesium rich deposits were less effective in reducing the rate for water reduction than were calcium rich deposits.

For the intermediate levels of crack tip stress intensity range examined using CT specimens, the two solutions produced similar crack growth rate data. Crack propagation rates were generally between 2 and 2.5 times faster under cathodic protection in seawater than in air. Significantly different fatigue behaviors were observed for the welded T-plates. Fatigue cracks initiated early within the specimens tested in natural seawater, but propagated at rates close to those observed in air. Synthetic seawater prolonged the initiation phase but gave rise to crack propagation rates that were about 2 times higher than those observed in air. These results have been explained in terms of the properties and precipitation kinetics of calcareous deposits.

Key words: calcareous deposits, cathodic protection, corrosion, fatigue, hydrogen embrittlement, seawater chemistry, steel, water reduction

TABLE OF CONTENTS

Page

ABSTRACT..... ii

LIST OF TABLES..... v

LIST OF FIGURES..... vi

NOTATIONS..... vii

1.0 INTRODUCTION..... 1

2.0 BACKGROUND - *Electrochemistry Within Fatigue Cracks Under Cathodic Protection in Seawater*..... 2

3.0 OBJECTIVES..... 8

4.0 EXPERIMENTAL PROCEDURES..... 10

4.1 Artificial Crevice Experiments..... 10

4.2 Compact Type (CT) Experiments..... 13

4.3 Welded T-Plate Experiments..... 15

Page

5.0 RESULTS 20

5.1 Artificial Crevice Experiments 20
5.1.1 Current Decay Transients 20
5.1.2 Tafel Plots 20
5.1.3 Deposit Analysis 21

5.2 Compact Type (CT) Experiments 23

5.3 Welded T-Plate Experiments 24
5.3.1 Crack Initiation Behavior 24
5.3.2 Crack Growth Behavior 25
5.3.3 Crack Profile Behavior 25
5.3.4 Behavior of Environmental Parameters 26

6.0 DISCUSSION - *Influence of Calcareous Deposits on Current Density and Fatigue Behavior* 34

9.0 CONCLUSIONS 29

10.0 SUMMARY 30

REFERENCES 49

APPENDIX 52

LIST OF TABLES

Table	Title	Page
1.	Chemical analysis and mechanical properties of G40.21 Grade 350 WT steel	32
2.	Water reduction data obtained from artificial crevice experiments	32
3.	Comparison of calcareous deposits found within artificial crevices polarized to -830 mV (SCE) at 5°C	33
4.	Linear regression analysis of CT data	33
5.	Chemical analysis of seawaters	34
6.	Overall Analysis of Results for Tests Conducted at 5°C and -830 mV (SCE)	34

LIST OF FIGURES

Figure	Title	Page
1.	Simplified illustration of the electrochemistry within a fatigue crack under cathodic protection in seawater	35
2.	Artificial crevice assembly	36
3.	Compact type (CT) specimen geometry	36
4.	Welded T-plate geometry	37
5.	Current decay transients for artificial crevices polarized to -830 mV (SCE) @ 5°C	38
6.	SEM analysis of calcareous deposits near tip of artificial crevice polarized to -830 mV (SCE) in 5°C synthetic seawater	39
7.	SEM analysis of calcareous deposits near tip of artificial crevice polarized to -830 mV (SCE) in 5°C natural seawater	39
8.	Comparison of fatigue crack propagation data for CT specimens tested in air with CT specimens tested at -830 mV (SCE) in natural and synthetic seawaters at 5°C	40
9.	Crack depth as a function of elapsed cycles for the welded T-plate specimens	41
10.	Comparison of cycles to initiation for the welded T-plate specimens	42
11.	Fatigue crack propagation rate as a function of crack depth for the welded T-plate specimens	43
12.	Comparison of ACPD readings with beach marks for the welded T-plate specimen tested in air	44
13.	Crack profiles for a welded T-plate specimen tested in 5°C synthetic seawater	45
14.	Crack profiles for a welded T-plate specimen tested in 5°C natural seawater	46
15.	Current decay transients for welded T-plates tested in 5°C seawater	47
16.	Distribution of particle size in 2 ml of solution for a 100 micron diameter aperture	48
17.	Distribution of particle size in 2 ml of solution for a 280 micron diameter aperture	48

NOTATIONS

a	crack depth
BFS	back face strain
da/dN	fatigue crack growth rate
E	electrochemical potential
f	cyclic frequency
i	current density
ΔK	crack tip stress intensity factor range
N	number of cycles
ΔP	applied load range
R	stress ratio or load ratio (minimum load/maximum load)
T	temperature

1.0 INTRODUCTION

In recent years, energy shortages have generated a drive towards the exploration, drilling and production of oil and gas in offshore environments. Many of the structures used in marine environments are made from carbon and low alloy steels. Even though such steels are susceptible to corrosion fatigue, they are widely used because of their relatively low cost and ease of fabrication. The primary concern is with the initiation and propagation of cracks in welded tubular steel intersections under cyclic loading in marine environments. Joints of this type usually contain weld defects which initiate fatigue cracks. The presence of such flaws eliminates much of the fatigue crack initiation period and fatigue life is usually governed by crack propagation from a weld toe into parent metal [1]. Since steels are subject to corrosive degradation in marine environments, the loss in fatigue resistance due to corrosion must be taken into account in engineering design. Designers, engineers and operators must be aware of the possible deleterious effects of environment-assisted fatigue on material performance and must assess the potential impact of these effects on the design, safety and reliability of offshore structures.

Before the severity of fatigue damage can be predicted for a given alloy in a marine environment, both the metal and the electrolyte must be understood. Until recently, more was known about the steel structures than about the seawater itself. Consequently, seawater has often been treated as an invariable fluid whose properties are well simulated by 3.5% NaCl solution. It was the intent of this study to investigate the influence of seawater chemistry on the electrochemical processes occurring within fatigue cracks and, in turn, on fatigue crack growth behavior. A knowledge of the electrochemistry within fatigue cracks under different combinations of bulk solution chemistry and environmental parameters is crucial to defining the mechanism(s) responsible for the enhanced fatigue crack growth rates observed for structural steels in aggressive solutions.

2.0 BACKGROUND - *Electrochemistry Within Fatigue Cracks Under Cathodic Protection in Seawater*

When steel is polarized cathodically in aerated seawater, two reduction reactions may take place on the metal surface: oxygen reduction and hydrogen reduction. The reduction of dissolved oxygen

$$O_2 + 2\,H_2O + 4\,e^- \;\Longrightarrow\; 4\,OH^-$$

is favoured kinetically for low cathodic over-potentials. Hydrogen reduction is possible via two different mechanisms, depending on the pH of the solution [2,3]. Under acidic conditions, the reduction of hydrated hydrogen protons

$$H_3O^+ + e^- \;\Longrightarrow\; H_{ads} + H_2O$$

is the charge transfer process responsible for hydrogen adsorption onto the steel surface. In neutral or alkaline solutions, as is the case in seawater (bulk pH 8.2), the reduction of H_2O species (water reduction)

$$H_2O + e^- \;\Longrightarrow\; H_{ads} + OH^-$$

is energetically favoured [3]. The adsorbed hydrogen atoms produced by this reaction may recombine to form hydrogen gas molecules, either by the chemical Tafel reaction

$$H_{ads} + H_{ads} \;\Longrightarrow\; H_{2\,(g)}$$

or by the electrochemical Heyrovsky reaction

$$H_{ads} + H_2O + e^- \;\Longrightarrow\; H_{2\,(g)} + OH^- \;.$$

Daft et. al [2] have shown that both of these recombination reactions occur simultaneously on iron electrodes. Of course, the adsorbed hydrogen atoms formed as an intermediate in the discharge step could, instead of recombining to form hydrogen gas, diffuse into the steel. Once absorbed into the metal, atomic hydrogen may diffuse to the highly stressed plastic zone located ahead of the crack tip where recombination can result in embrittlement.

Any process that produces atomic hydrogen at the surface of a metal will normally induce considerable hydrogen absorption into the metal. When steel is charged cathodically, there is an equilibrium established between adsorbed atomic hydrogen on the external surface and hydrogen atoms in solution in the metal. A similar equilibrium exists between hydrogen adsorbed on internal surfaces and molecular hydrogen formed in microvoids [4]. For the solubilities normally encountered in steels, this equilibrium pressure could be as high as 200,000 psi [5]. When interstitially dissolved hydrogen atoms come into contact with an internal surface, they will tend to diffuse out and recombine to form molecular hydrogen until the pressure of the gas has reached a value in equilibrium with the remaining lattice hydrogen. When the internal surface is located deep within, the large mass of metal surrounding the defect prevents significant plastic deformation and cracking results [5].

It is unlikely that significant anodic dissolution could occur by the simple mechanism

$$Fe \;\Longrightarrow\; Fe^{2+} + 2\,e^{-}$$

for external potentials more negative than about -800 mV vs. SCE (complete corrosion protection is possible at potentials more negative than -780 mV vs. SCE) and, hence, hydrogen embrittlement is probably the dominant mechanism operating to produce the enhanced crack growth rates often observed for structural steels under cathodic protection in seawater.

Evidence in support of a hydrogen embrittlement mechanism for the accelerated fatigue crack growth rates found in structural steels under cathodic protection in marine environments has been accumulating rapidly in recent years. To begin with, it should be pointed out that the hydrogen embrittlement mechanism associated with fatigue cracking is a time-dependent phenomena. The severity of hydrogen embrittlement in steels is highly dependant upon the rate of diffusion of hydrogen into the tri-axially stressed region ahead of the crack tip. It has been argued that the maximum effect of the environment on the crack growth rate will not be seen unless sufficient hydrogen has had time to accumulate in this region of high tri-axial stress [6]. Consequently, the influence of absorbed hydrogen atoms on fatigue crack growth behavior will depend on crack growth per unit time rather than on crack growth per cycle.

Vosikovsky et al. have demonstrated that slower cyclic frequencies [7] and warmer temperatures [8] both result in substantially higher 'plateau' (i.e. ΔK independent) crack growth rates. As the cyclic frequency is increased, the rate of supply of adsorbed hydrogen becomes limited at lower values of ΔK because crack growth is faster on a time basis. Since hydrogen adsorption [9], absorption [10] and diffusion [11] all increase with temperature, a higher plateau crack growth rate would be expected at room temperature than at 0°C. Cottis et. al [11] have shown that the hydrogen permeation current for a low carbon steel approximately doubles for every 10°C rise in temperature. It is probably no coincidence that Vosikovsky et. al [8] have measured plateau crack growth rates for cathodically polarized steel specimens that were about four times slower at 0°C than at 25°C. With decreasing testing temperature or increasing strain rate, hydrogen diffusion is less able to keep up with the propagating crack front and the severity of embrittlement decreases until it is not observed at all [12].

Scott et al. [13] recognized that hydrogen embrittlement could be an important factor in fatigue crack growth behavior and suggested that, for the case of plateau crack growth, the supply of hydrogen becomes rate limiting. Plateau rates of crack growth were correlated with the cathodic protection potential and it was concluded that the hydrogen/water reduction reaction, under activation control at the crack tip, was the important rate determining step.

Fractographic examination of the fracture surfaces produced in fatigue specimens of structural steels cathodically polarized in seawater provides additional evidence. Scott [6] has found numerous cleavage planes on the fracture surfaces of cathodically protected BS4360 Grade 50D steel specimens, corresponding to ΔK values between 10 and 30 $MPa \cdot m^{1/2}$ (where 'plateaus' normally appear). Maahn [14,15] has reported that lowering the protection potential from -800 to -1200 mV (SCE) increases hydrogen uptake by a factor of about 25 and has associated the higher crack growth rates observed for more negative cathodic potentials with an increasingly brittle fracture appearance of fracture surfaces.

The cathodic reduction of dissolved oxygen and/or water molecules on steel surfaces acts to increase the pH of the electrolyte immediately adjacent to the metal. The reason being that both of these reactions result in the production of hydroxyl ions. In seawater, an increase in pH for the electrolyte adjacent to a steel surface also results in the

formation of hard, dense mineral deposits (commonly termed 'calcareous deposits'), rich in calcium and/or magnesium (Figure 1, p.35).

Several researchers [8,13,16,17] have measured fatigue crack growth rates at low stress levels under cathodic protection in seawater that are actually slower than the rates measured in comparable air tests. It has been reasoned that a reduction in the 'effective' stress intensity range, due to the precipitation of calcareous deposits inside the crack, is the mechanism responsible for such crack growth retardation. The calcareous deposits were observed to cause the minimum value of measured crack opening to increase while the maximum value remained virtually unchanged [13,17]. It has also been suggested that calcareous deposits might exert a strengthening influence in the crack tip vicinity [16].

It is possible that a third mechanism may also be contributing to crack growth retardation under cathodic protection at low values of crack tip stress intensity range, ΔK. The deposition of insoluble mineral deposits on the crack walls could lead to a depletion of reactants (e.g. water) at the metal surface. Less adsorbed hydrogen on the crack faces would mean a slower diffusion rate for hydrogen into the metal and less damage brought about by the mechanism of hydrogen embrittlement.

The effectiveness of calcareous deposits in limiting the production of H_{ads} on the crack surfaces will depend upon the 'quality' of the mineral deposits formed there. Even though calcareous deposits have been generated under the influence of cathodic protection for years, until recently, relatively little information has been published concerning the delicate relationship existing between deposit properties and the conditions under which they form. Temperature, electrolyte velocity (flow rate), dissolved oxygen concentration, protection potential and seawater chemistry and are now known to influence the chemistry and properties of these mineral deposits.

Calcareous deposition is, undoubtably, a nucleation and growth process that strongly depends upon the above parameters. Several of these variables, namely flow rate, dissolved oxygen concentration and potential are inter-related since they all affect the cathodic current density and pH profile at the metal-solution interface. Probably the most important single feature of a calcareous deposit is its ratio of calcium to magnesium. The 'protective' nature of the deposit depends upon this ratio which, in turn, is a function of seawater chemistry, temperature and most importantly, the pH profile generated at the steel

surface. Changes to this system of parameters will change the relative amounts of calcium carbonate and magnesium hydroxide incorporated into the deposit and affect its quality.

The magnitude of impressed current used to polarize the steel surface probably exerts the greatest influence on deposit chemistry and properties. The higher the cathodic current density, the greater the electrolyte pH adjacent to the metal surface and, as a result, the thicker the calcareous film [18]. A higher pH at the metal surface also decreases the Ca:Mg ratio of the deposits because precipitation of $Mg(OH)_2$ in seawater at 5°C requires that the pH be greater than 10.6 [19], whereas seawater is supersaturated with calcium ions at the ambient pH of 8.2 [20].

Limited information regarding the effect of magnesium ions on deposit formation and properties has been reported by Culberson [21]. Tests carried out in artificial seawater at 25°C clearly demonstrate that the long term current density requirement for cathodic protection at a set potential is greatly increased by the presence of magnesium ions. Two deposits were formed: one with magnesium ions in solution and one without. The deposit that formed in the absence of magnesium ions developed more rapidly and resulted in a final current density that was thirty times lower. Ambrose et. al [22] have suggested that areas of low electrical resistance contain high concentrations of magnesium hydroxide and correspond to sites where cathodic current density is high. Rapid hydroxide production favours the precipitation of magnesium hydroxide over calcium carbonate and these locations remain as potential defect sites where damage due to hydrogen embrittlement is a real possibility.

Habashi et. al [23] have studied the deposition kinetics of calcareous deposits and found that precipitation started with pure magnesium compound and gradually changed to a stable Ca:Mg ratio after approximately 17 hours. This stable ratio showed a dependance on potential, changing from pure calcium compound at -950 mV (SCE) to pure magnesium compound at -1100 mV (SCE). These observations are consistent with the opinion of Preiser et. al [24], who have suggested that the magnesium compounds form an amorphous matrix which functions as a bonding agent from which microcrystalline calcium-rich constituents are suspended.

Lucas et al [25] have monitored the hydrogen permeation rates in BS 4360 Grade 50D steel membranes under cathodic protection in 3.5% NaCl solution and in artificial

seawater. In the sodium chloride solution, the hydrogen permeation transients increased with decreasing potential. In contrast, hydrogen absorption was observed to decrease during the test in seawater, despite successive lowering of the control potential. At -1150 mV (SCE), the hydrogen permeation rate was ninety times higher through the steel membrane tested in the sodium chloride solution. The lower permeation currents observed in seawater were attributed to the formation of a calcareous deposit about 50 μm thick. The generation of cracks in the surface deposit, possibly as a result of hydrogen gas evolution, caused temporary increases in hydrogen permeation. Analysis of the deposit showed that it was rich in both calcium and magnesium compounds.

3.0 OBJECTIVES

The Ocean Engineering Group of the Faculty of Engineering and Applied Science at Memorial University is currently involved with the University of Waterloo and the Physical Metallurgy Research Laboratories of CANMET in a fatigue research program on large scale welded tubular joints fabricated from structural steel. Two solutions, ASTM substitute ocean water (synthetic seawater) and natural seawater, are used more or less interchangeably to predict the fatigue crack growth properties of steels. There is evidence (refer to background information) to suggest that the mechanism responsible for accelerated fatigue crack growth in medium strength structural steel cathodically protected in seawater (i.e. water reduction) can be significantly influenced by bulk solution chemistry. Carefully planned experiments were therefore necessary to investigate the relative severity of these two solutions when used with cathodically protected steel samples. The investigation was conducted using three different specimen types:

1.) Artificial Crevices
2.) Compact Type (CT) Specimens
3.) Welded T-Joints

The steel and weld material used to make each of these specimens conformed to the same specifications as those used to make up the welded tubular T-joints.

The major objective of the research was to establish the relative severity of natural and synthetic seawaters on the fatigue behavior of welded plate T-joints subjected to the same conditions of stress, temperature and cathodic protection as the larger welded tubular T-joints being tested under the current program.

A secondary objective was to investigate the influence of calcareous deposits on water reduction kinetics and fatigue crack growth behavior. The bulk of the research already conducted on these deposits deals with external surfaces. At present, there is little in the way of data characterizing the composition and properties of deposits that form within crevices or cracks. It has been recognized that calcareous deposition within fatigue cracks can influence crack propagation rates. Calcareous deposits may provide protection against hydrogen adsorption onto steel surfaces and subsequent hydrogen embrittlement. Since the chemistry of calcareous deposits is substantially dependent upon current density,

it would seem reasonable that a relationship between the type of calcareous deposit and the amount of water reduction (the source of atomic hydrogen responsible for hydrogen embrittlement) could be established. Once such a relationship has been realized, a reasonable estimate might be possible with regard to the magnitude of water reduction occurring within a fatigue crack based on the type of calcareous deposits found on the fracture surfaces and a knowledge of the electrochemical potential history of the specimen.

Artificial crevices were used to study the morphology of calcareous deposits and their influence on water reduction kinetics. The principle advantage of using artificial crevices to study calcareous deposition lies in their small size and ease of disassembly. Upon completion of a test, the two surfaces can be quickly separated and transported to the scanning electron microprobe without risking damage to the deposits from sectioning the steel. A major disadvantage of the artificial crevice is that it does not simulate the alternate opening and closing of the fatigue crack during a stress cycle. Restricted circulation of the solution within an artificial crevice might affect the pH profile and deposit morphology. However, the main objective behind the artificial crevice experiments was to obtain a relationship between calcareous deposit chemistry and the rate for water reduction on the steel's surface. If such a relationship exists, it should remain valid regardless of the conditions under which the deposits are formed.

Compact type (CT) specimens were tested to obtain crack tip stress intensity factor range versus crack growth rate (log ΔK vs. log da/dN) data for the different seawater solutions, since it is difficult to derive similar curves from welded T-plate data.

4.0 EXPERIMENTAL PROCEDURES

Experimental procedures for the artificial crevice, CT and welded T-plate experiments are discussed individually in the following sections. The same steel was used in the fabrication of all three specimen types. It is control rolled and normalized G40.21 Grade 350 WT. The composition and mechanical properties of the steel are listed in Table 1 (p.32).

In order to prevent contamination of the seawater solutions, only inert (non-corrosive) materials were used in the fabrication of seawater enclosures and circulation systems. Upon completion of testing, specimens were rinsed thoroughly in distilled water and dried with acetone to prevent atmospheric oxidation of the surfaces before photographs could be taken.

Filtered, natural seawater was supplied free of charge by Memorial University's Marine Lab located at Logy Bay, Newfoundland. The required quantities of synthetic seawater (including heavy metal additions) were made according to ASTM standard D1141-75 (1980), using distilled water and reagent grade chemicals.

4.1 Artificial Crevice Experiments

Two independent electrochemical cells were used to immerse artificial crevice specimens in solutions of synthetic and natural seawater. The temperature was controlled by placing both cells in an ice-chest containing glycol. Cooling was provided by an MGM Lauda Brinkman model B-2 refrigeration unit with adjustable temperature control. Air entering the electrochemical cells was pre-cooled by routing it through a small coil of copper tubing immersed in the glycol.

The samples were placed under potentiostatic control using a Polarographic Analyzer model 2A and a university fabricated potentiostat model ENR-01-EE. Current was monitored by placing 0.5 watt capacity 1000 ohm resistors in line with the counter electrodes. The voltage drop across each resistor was measured by a Fluke Digital

Multimeter model 8000A. Knowing the exposed area of the specimen (2.0 cm^2), the current density could be determined for each sample.

Scanning Electron Microscopy (SEM) with Energy Dispersion X-Ray Analysis (EDAX) was used to study the morphology and composition of calcareous deposits that formed on the exposed surfaces. In order to keep the steel specimen from charging under electron bombardment during SEM-EDAX analysis, the calcareous deposits were sprayed ahead of time with a carbon coating.

The artificial crevices were constructed from two pieces of steel fixed together with a nylon bolt, yet separated with sufficient electrical tape to give a crevice 1 cm wide, 1 cm deep and 0.20 mm in height (Figure 2, p.36). The two halves were electrically connected by spot welding a copper clad stainless steel probe across the back faces of the specimen.

Surface preparation consisted of abrasion with silicon carbide paper down to 600 grit. The surfaces were rinsed with distilled water between each grit. After the final abrasion, the surfaces were once again rinsed with distilled water, then degreased and dried using acetone in order to prevent premature corrosion of the surface. Following surface preparation the specimen was assembled. The outer surfaces of the sample were made inert by coating with Devoe 235 Marine Epoxy. The sides were sealed using silicone. The only exposed areas were the top and bottom surfaces of the crevice, each measuring 1 cm^2 for a total exposed area of 2 cm^2. In order to wet the exposed surfaces of the crevice, seawater (from a wash bottle filled with the appropriate solution) was injected into the mouth of each specimen before placing it into its electrochemical cell.

Tests were conducted under potentiostatic control at -830 mV (SCE) in natural or synthetic seawater solutions maintained at 5°C. Current density readings were recorded periodically over the duration of the test (approximately three weeks).

Data for Tafel plots was gathered over a 45 minute period at the end of the three week experiment, immediately before the samples were removed from their electrochemical cells. The potential was then stepped from the setting used during the experiment, down to -1150 mV (SCE), in increments of 25 mV. The specimens were held at each potential for a sufficient length of time (usually between three and five minutes) to allow the current densities to stabilize before taking measurements. As the potential of a specimen is

continually decreased, the rate for dissolved oxygen reduction becomes diffusion limited and a greater percentage of the overall reduction rate is due to water reduction. As the readings progress negatively beyond about -1000 mV (SCE), any increase in current density is almost entirely a result of water reduction.

The reduction reaction rates are known to obey a logarithmic (Tafel) relationship as a function of electrochemical potential. In cases where the potential is more negative than that for the reversible hydrogen electrode, the overall reduction reaction is a combination of both oxygen reduction and water reduction. Under such conditions, a logarithmic increase in current density is an additive result of a logarithmic increase in current density for water reduction and a logarithmic increase in current density for oxygen reduction for each linear increase in potential. However, if the amount of dissolved oxygen available for oxygen reduction is restricted, then the resulting increase in reaction rate is less than that predicted by the Tafel relationship (for a given linear increase in potential). This shows on the plot as a curve. As the potential is further increased and the supply of dissolved oxygen becomes depleted, the amount of oxygen reduction contributing to the overall reduction reaction becomes negligible. After this point, any increase in the reduction reaction rate is a direct result of an increase in water reduction. Since the water reduction reaction rate is independent of dissolved oxygen concentration, any increase in reaction rate will reflect the Tafel relationship. This is evident in the Tafel plot by a straightening out of the curve. Once this section of each plot has been established, a comparison of water reduction rates is possible.

The rates for water reduction occurring under various experimental conditions with existing calcareous films can be compared with those determined under similar conditions for film-free surfaces. Additional Tafel plots for film-free artificial crevices and for film-free, boldly exposed (external) surfaces of the same steel were generated for comparison with the Tafel plots obtained for crevices having calcareous scales. Specimens were prepared according to the same procedure. Tafel plots for film-free surfaces were obtained immediately after immersion of the specimens in de-aerated solutions. A nitrogen purge was used to maintain a low concentration of dissolved oxygen within the cells.

4.2 Compact Type (CT) Experiments

The CT specimens used in these tests were cut from one inch steel plate and machined to the dimensions shown in Figure 3 (p.36). The specimens were fabricated such that the fatigue crack propagated perpendicular to the rolling direction. An MTS 850 Material Test System gave strict control over the loading program and kept accurate count of elapsed cycles. The loading frame was contained in a refrigerated cold room and temperature was monitored using an Omega Model 199 Thermocouple Indicator with a copper/constantan thermocouple junction.

For tests conducted in air, crack depth was measured using a type 2152 travelling optical microscope manufactured by The Precision Tool & Instrument Company. For tests conducted in seawater, a strain gage, centered on the back face of each specimen and wired to a Bruel & Kjaer Type 1526 Strain Indicator was used to measure crack depth. A temperature compensation gage helped to eliminate drifting strain readings due to temperature fluctuations in the cold room.

The seawater enclosure used to house the specimen was constructed from half-inch lexan, a clear rigid plastic with great fracture resistance. Ports were included for the attachment of inlet and outlet circulation hoses and for the insertion of a platinum wire counter electrode and a saturated calamel reference electrode (SCE). Seawater from a 20 liter Nalgene holding tank was fully aerated and circulated through the enclosure at approximately 1 liter/min by means of a variable speed, magnetically coupled, centrifugal pump. The electrochemical potential of the specimen was controlled to within two millivolts of the set potential by a PAR model 173 Potentiostat.

All specimens were degreased with acetone and polished along the back face. It was important to have a smooth, flat surface at this location to ensure good adhesion and proper functioning of the strain gage. For tests conducted in air, it was necessary to polish the specimen in the region of crack propagation. A smooth, shiny surface is essential for detection of the crack tip under a travelling microscope.

For tests conducted in seawater, optical readings were not taken. The entire specimen was coated with urethane to reduce the current required for cathodic protection. Both sides of the specimen were coated with silicone in the region of crack propagation to

prevent the cross flow of solution from interfering with fatigue crack growth behavior. Additional coatings were applied to the strain gage to help resist exposure to the seawater. Finally, a short piece of copper coated, stainless steel wire was spot welded to the top surface of each seawater specimen to facilitate attachment of the working electrode lead coming from the potentiostat.

The CT specimens were designed to produce crack growth rate data for the intermediate levels of crack tip stress intensity range between about 15 and 30 MPa•$m^{1/2}$. All specimens were pre-cracked in room temperature (22°C) air using a sinusoidal cyclic frequency of 20 Hz and a load reduction technique that began with a 20 KN load range and ended with a 10 KN load range after 15 mm of crack growth. The load range was reduced in 20% increments after allowing for sufficient crack extension to take place at each load level. A load ratio of 0.5 was maintained at all times.

Before conducting experiments in seawater, it was necessary to establish a relationship between back face strain (BFS) and crack depth for the specimen geometry and load range used in these tests. For this purpose, and to provide a basis for the comparison of fatigue growth rate data for different solution chemistries, three specimens were tested at 20 Hz (sinusoidal) under a 10 KN load range and a 0.5 load ratio in 5°C air. The tests began when the crack was 15 mm in length and ended after it propagated to a length of 33 mm (after 33 mm, the specimen size requirements become violated). Minimum and maximum BFS readings were recorded and the corresponding crack depths measured optically at approximately 1 mm intervals. The total cycle count was also recorded for each crack depth.

Computer software was used to generate a third order polynomial curve fit through the air test data. The following equation was found to relate maximum BFS (BFS_{max}) to crack depth (as measured from the machined notch tip):

$$\text{crack depth} = 2.806\times10^{-9}(BFS_{max})^3 - 1.672\times10^{-5}(BFS_{max})^2 + 3.838\times10^{-2}(BFS_{max}) - 0.3714$$

Using this relationship, it was possible make accurate measurements of crack depth within CT specimens tested in seawater.

Altogether, five CT specimens were tested in seawater solutions maintained at 5°C: three in natural seawater and two in synthetic seawater. A third test in natural seawater was

necessary after a strain gage malfunction occurred about halfway through one of the tests. All tests in seawater were conducted under cathodic protection at -830 mV (SCE). Each specimen was rinsed in distilled water and dried with acetone immediately upon completion of the test.

Crack depth vs. cycles data for each specimen were converted to crack growth rate vs. crack tip stress intensity range data using a computerized, seven point incremental polynomial technique and plotted against a standard log-log scale. Linear regression analysis was used to determine values for "C" and "m" of the Paris equation for the various experimental conditions studied.

4.3 Welded T-Plate Experiments

Five 19 mm T-plates with identical overall geometries (Figure 4, p.37) were welded to the same specifications. The attachment plate was fastened to the base-plate by full penetration manual arc welding with 7018, low-carbon, low-hydrogen welding rods. None of the five T-plates were pre-heated and no restraint was applied during welding. After welding, one of the weld toes was shallowly ground with a pencil grinder to ensure that the crack developed on the instrumented, unground weld toe.

After the weld toe grinding operation, each T-plate was first wire-brushed to free it of rust, loose mill scale and dirt and then degreased with a general purpose solvent. Twenty sets of equally spaced copper clad stainless steel wire (ACPD) probes were tack welded along the unground weld toe. Two coats of Devoe 235 marine epoxy paint were applied to all surfaces excluding the area immediately adjacent to and including the weld beads on the instrumented side of the T-plate. The area of uncoated steel measured approximately 100 cm^2. When the epoxy was dry, shielded coaxial cables were soldered to each pair of ACPD probes. The plates were then inserted into their respective loading frames, checked for proper alignment and secured in place using end clamping brackets and a single pin connection.

The loading system consisted of an electro-hydraulic Material Test System (MTS), its associated framework, and the frames which held the T-plates. The T-plates were subjected to a tension to tension, constant amplitude, sinusoidal load in 3-point bending. A

weld toe stress range of 150 MPa, a cyclic frequency of 0.2 Hz and a load ratio of 0.05 were used in all seawater tests. The loading program for the air test was identical to that of the seawater tests except for the cyclic frequency. Since environmental factors are not a consideration in air testing, it is permissible to operate at a higher frequency (3 Hz) in order to save time.

A Hewlett-Packard data acquisition system was used to obtain, store and analyze all the necessary information. Two major software packages were developed. The first and most important was the data acquisition program. This program automatically obtained, printed and stored measurements of crack depth, strain, temperature, dissolved oxygen concentration, pH, supplied current and reference potential. A separate plotting software package was developed for data analysis. Programs were written to illustrate crack profiles at different stages of crack growth and provide graphs of crack depth versus cycles, crack growth rate versus crack depth and current density versus cycles.

Determination of strain levels at various positions on the instrumented side of the base-plate was accomplished using type M&M EA-06-125AD-120 precision strain gauges and a Vishay Instruments strain gauge conditioning system.

Crack depth was monitored using a Model U7G Crack MicroGauge. The operation of this instrument is based on an AC potential drop (ACPD) technique. A high frequency AC field is applied across the weld toe by means of shielded field lead wires. Active and reference probe pairs are situated near the weld toe. The active pair spans the weld toe whereas the reference pair does not. In the absence of a crack, there is an initial potential drop across each pair: v_1 across the active pair and v_2 across the reference pair which satisfies the following equation:

[1] $r/v_2 = c/v_1$ where r = reference probe separation
c = active probe separation

After a crack develops at the weld toe, v_1 will have changed to v_1' while v_2 will have remained nearly the same at v_2'. This increase in v_1 is due to the AC field having to conform to the surface of the steel because of its high frequency. Since the crack effectively increases the surface distance between the active probe pair, the resistance along that path is

greater and consequently the voltage drop is greater. This increase in effective surface distance is related to the voltage drop by the following equation:

[2] $r/v_2' = (2a+c)/v_1'$ where a = (increase in distance)/2
= crack depth

Combining [1] and [2] and solving for a gives:

[3] $a = (c/2)(v_1'/v_2' - v_1/v_2)$

which is the equation used in the data acquisition software to solve for crack depth.

Prior to plotting, a must be operated on by a calibration function to give the actual crack depth:

[4] $a_{actual} = f(a)$ where $f(a)$ = calibration function
$= -4.474\text{x}10^{-2} + 1.523a - 3.612\text{x}10^{-2}a^2$

This operation is performed by the plotting software. The calibration function was obtained from a regression analysis of ACPD data collected from several air tests on similar specimens, by a co-worker. With this technique, cracks as small as 0.2 mm could be detected and deeper crack depths ascertained to within ±1 mm.

Measurement of dissolved oxygen content and temperature was accomplished with a Precision Scientific Galvanic Cell Oxygen Analyzer (GCOA). One dissolved oxygen probe was positioned in each holding tank in close proximity to the outlet hose. Temperature measurements were obtained using thermistors (calibrated temperature sensitive resistors) whose leads were connected to the rear of the GCOA.

A Metrohm-Herisau model E488, full range analog pH meter with adjustable calibration controls was used to monitor seawater pH during each test. Calibration of the instrument was checked periodically using buffer solutions of pH4 and pH10.

The T-plates were cathodically protected using specially built potentiostats and copper/copper sulfate reference electrodes. Each potentiostat was equipped with front panel

jacks that were connected directly to the data acquisition system for periodic measurement of the reference potential and supplied current.

Two independent but identical circulation systems, each consisting of a lexan seawater enclosure, circulation pump and assorted tubing and connectors provided the necessary supply of seawater to each T-plate. Two plastic (Xactics) holding tanks were used to contain the bulk of the seawater and insulate it from the warmer surroundings. A large (1000 L) tank held the synthetic seawater while a smaller (750 L) tank contained the natural seawater.

Two miniature bilge pumps were used, initially, to pump the seawater from the enclosures back to the holding tanks. However, after only two to three weeks of service, the pumps failed and were subsequently replaced by two Cole Parmer model OEM miniature gear pumps. The pumps were controlled by a two channel, variable power supply. The circulation rate was established by adjusting the pump speed, while a float controlled, level sensing input valve regulated the water level in each enclosure. The cooling system comprised a Tecumseh model AH7480AC refrigeration unit and two 316 stainless steel cooling coils. External thermostats, one for each holding tank, were used to control the flow of refrigerant as demanded.

Two T-plates were tested in synthetic seawater and two in natural seawater. One T-plate was tested in air. The seawater tests were conducted at 5±2°C in oxygen saturated solutions with circulation rates close to one liter per minute. An electrochemical potential of -900 mV vs. $Cu/CuSO_4$ (equivalent to -850 mV vs. Ag/AgCl in seawater or -830 mV vs. SCE) was employed in all four seawater tests. It was decided to perform the air test upon completion of the first two seawater tests, while one of the hydraulic actuators underwent repairs to an oil leak. The air test provided data for checking the accuracy of the ACPD readings and served as a basis for comparing the seawater tests.

Measurements were taken daily until crack initiation and twice daily until failure. Before taking measurements, load cycling was stopped on both MTS channels so that mean loads were applied to each T-plate. Printouts of all data were obtained and stored as safeguards against disk failure.

The ACPD measurements were used to generate crack profiles at various stages of crack growth, produce plots of crack depth vs. cycles and determine crack growth rates as a function of crack depth. Crack growth rate data were calculated from the crack depth vs. cycles data using a computerized, seven point incremental polynomial technique. A faulty connection to the Crack MicroGauge Unit prevented the retrieval of any useful ACPD data from the first test in natural seawater. Although crack profiles could not be generated for this plate, it was possible to obtain information on its crack propagation behavior from a correlation of actuator displacement at mean load with maximum crack depth. Transducer outputs from the MTS were recorded in conjunction with each set of data measurements for all five T-plates. The displacement of the actuator at mean load was determined by subtracting the mean stroke reading at the start of the test from subsequent mean stroke indications as the test progressed. Since semi-elliptical fatigue cracks usually form relatively straight fronts soon after initiation, ACPD data from the four probe sets closest to the center of the crack were averaged for three of the four remaining T-plates to give crack depth as a function of actuator displacement at mean load. A linear correlation was established between crack depth and actuator displacement at mean load and this relationship was then used to generate crack depth vs. cycles data for the first test in natural seawater.

5.0 RESULTS

5.1 Artificial Crevice Experiments

5.1.1 Current Decay Transients

The artificial crevice specimen placed in synthetic seawater maintained a consistently higher current density throughout the duration of the test (Figure 5, p.38). In both solutions, the current densities varied noticeably during the first 150 hours but thereafter stabilized at levels close to the initial measurements. The stable current density achieved within synthetic seawater (7 uA/cm^2) was substantially higher than that achieved within natural seawater (4 uA/cm^2).

5.1.2 Tafel Plots

Tafel plots, comparing the rates for water reduction under different environmental conditions have been included as an appendix. The key information available from the Tafel plots is summarized in Table 2 (p.32). The rates for water reduction varied considerably among the different specimens. Tafel slopes ranged from 115 to 225 mV/decade. The Tafel slope most commonly measured for iron in chloride solutions is 120 mV/decade [26]. The different values observed here probably reflect variations in temperature, specimen geometry, solution chemistry and surface deposits. The Tafel slopes were determined by drawing tangents to the curves at their flattest locations. Flattening out usually occurred between -1000 and -1150 mV (SCE). Above -1000 mV, oxygen reduction contributes significantly to the current density and below -1150 mV, the generation of hydrogen gas tends to reduce the active surface area. Both of these effects were more pronounced with crevice specimens than with external surfaces. In order to evaluate the effects of temperature, specimen geometry, solution chemistry and surface deposits on the rate for water reduction, the Tafel slopes were extrapolated back to a common potential and the corresponding current densities recorded. The potential chosen for this purpose was -830 mV (SCE), the same potential use for protecting the CT specimens and welded T-joints.

Consider first, the results obtained for film-free (i.e deposit-free) surfaces. The current density for water reduction was 2.7 times higher in natural seawater than in synthetic seawater for the boldly-exposed surfaces. Within the film-free crevices, current densities were only slightly higher for natural seawater than for synthetic seawater.

Consider next, the effect of surface films on water reduction kinetics within the crevices. In both tests, the rate for water reduction was reduced, more or less, by the presence of calcareous deposits. The deposits which formed within the crevice tested in natural seawater reduced the current density by a factor of 19. In comparison, the calcareous deposits which precipitated within the crevice tested at the same potential and temperature in synthetic seawater produced only a 5 fold reduction in current density. It is apparent that, for a cathodic protection potential of -830 mV (SCE) and a temperature of 5°C, calcareous deposits which precipitate within crevices exposed to natural seawater afford better protection against water reduction than deposits which precipitate within crevices exposed to synthetic seawater .

5.1.3 Deposit Analysis

Scanning Electron Microscopy (SEM) with Energy Dispersion X-Ray Analysis (EDAX) was employed to examine the morphology and composition of calcareous and/or corrosion products that precipitated on the crevice surfaces. Both the morphology and chemistry of the deposits differed significantly for the different bulk solution chemistries. Table 3 (p.33) provides data on the chemical composition of calcareous deposits that formed within the crevices. Deposits were sampled near the mouth, center and tip of each crevice for both the top and bottom surfaces (Figure 2, p.36). The ratio of calcium to magnesium was determined for each location sampled.

The crevice exposed to synthetic seawater formed a film of magnesium rich deposit over its entire surface. The deposit thickened and displayed a higher density of shrinkage cracks towards the crevice tip (Figure 6, p.39). The fact that the deposits thickened towards the crack tip is evident from the increasing percentage of magnesium and decreasing percentage of iron indicated in the analyses as the deposits were probed from the crevice mouth towards the tip (Table 3). Calcium concentrations were extremely low at all locations

and there were no signs of corrosion within the crevice. Deposits which formed within the crevice exposed to natural seawater did not provide complete surface coverage and differed significantly in physical appearance and chemical make-up (Figure 7, p.39). The crystal buds seen in Figure 7 were individually probed and found to be extremely rich in calcium. The calcium content of these deposits was found to increase towards the crevice tip and this is indicated by the increasing ratio of calcium to magnesium in Table 3. The high iron count present in these analyses reflects the lack of surface coverage afforded by the deposits. The high iron concentrations are thought to result from the substrate steel rather than from within the deposit.

5.2 Compact Type (CT) Experiments

Plots of crack growth rate (da/dN) versus crack tip stress intensity factor range (ΔK) were determined for each test. The results are compared in Figure 8 (p.40). Data for the air tests was included to serve as a base line for comparing seawater tests. Table 4 (p.33) gives values for C and m of the Paris-equation, derived from a linear regression analysis of the CT data.

The crack growth rate data for tests conducted in air appear reasonably linear over the range of ΔK examined. The scatter in data was small for $\Delta K<20$ MPa$\cdot$m$^{1/2}$, but increased slightly for $\Delta K>20$ MPa$\cdot$m$^{1/2}$, where crack growth rates deviated by as much as 25% for the same ΔK.

Only subtle differences in crack growth rates were apparent for the two seawater solutions and these differences were only observed for $\Delta K>20$ MPa$\cdot$m$^{1/2}$. Tests conducted in natural seawater produced crack growth rates that were, on the average, about 2 times faster than those observed in air. Fatigue cracks propagating in synthetic seawater grew about 2.5 times faster than cracks which grew in air. However, the scatter band associated with the seawater tests for $\Delta K>20$ MPa$\cdot$m$^{1/2}$ is of the same order of magnitude as that determined for the air tests (i.e. 25%). Thus, it would seem improper to attach special significance to the slightly higher crack growth rates observed for synthetic seawater.

There is evidence of plateau (constant) crack growth over a small range of ΔK corresponding to 4.5×10^{-5} mm/cycle for natural seawater and 5.5×10^{-5} mm/cycle for

synthetic seawater. The short plateaus observed here are, no doubt, a consequence of the relatively high starting value for ΔK (15 MPa·m$^{1/2}$). A smaller starting value for ΔK (say 10 MPa·m$^{1/2}$) might have produced wider plateaus, but would also have extended the test duration significantly. There was no evidence of calcareous deposition on the fracture surfaces of any of these specimens.

5.3 Welded T-plate Experiments

5.3.1 Crack Initiation Behavior

There was a considerable influence of seawater chemistry on fatigue crack initiation (Figures 9 and 10, p.41-42). The crack depths plotted in Figure 9 were determined by averaging the four ACPD probe set readings closest to the center of the crack. Thus, for cracks with high aspect ratios (a/c = maximum crack depth/half width), the average crack depth may be slightly lower than the maximum. Both specimens tested in natural seawater initiated cracks faster than did the specimen tested in air. The T-plate broken in air initiated a detectable crack after approximately 300,000 load cycles. The first T-plate tested in natural seawater (NATURAL#1) started cracking after only 90,000 cycles and a fatigue crack was detectable in the second T-plate tested in natural seawater (NATURAL#2) after about 150,000 cycles. Both specimens tested in synthetic seawater exhibited delayed initiation. In fact, only the first specimen tested in synthetic seawater (SYNTHETIC#1) actually grew a crack, which initiated after about 400,000 cycles. The second T-plate tested in synthetic seawater (SYNTHETIC#2) lasted through more than 1,000,000 cycles without developing a fatigue crack. Two separate probe sets, located near the center of the plate, indicated steadily increasing crack depth up to 0.3 mm over approximately 500,000 cycles, but did not increase further. All other probe sets produced readings less than ±0.1 mm.

5.3.2 Crack Growth Behavior

Major differences in crack growth rates for the two solutions and for air were also evident (Figure 11, p.43). The crack growth rate for the air test increased fairly linearly with crack depth. Crack growth rates for the seawater tests increased rapidly during the

early stages of crack growth, then leveled off. On the whole, synthetic seawater produced crack growth rates that were between 2 and 3 times faster than those observed in the air test, whereas cracks growing in natural seawater propagated at rates much closer to those observed in air. For crack depths less than about 2 mm or greater than about 4 mm, crack growth was slightly faster for NATURAL#1 than for NATURAL#2. For crack depths between about 2 and 4 mm, da/dN was between 1.5 and 2 times faster in both natural seawater specimens than in air. The crack growth rates for both natural seawater specimens became relatively constant for depths greater than about 4 mm. The crack growth rate for the air test did not. For crack depths greater than about 8 mm, da/dN for air is seen to rise above that for natural seawater. The crack growth rate for the specimen tested in synthetic seawater did not level off until the crack depth was greater than about 7 mm. The crack growth rate at this depth was about 2 times faster in synthetic seawater than in natural seawater.

5.3.3 Crack Profile Behavior

Crack profiles, as a function of elapsed cycles, for the air test and for two of the seawater tests are presented as Figures 12-14 (p.44-46). Figure 12 compares ACPD data (after modification using the calibration function discussed earlier) with beach marks for the air test. The ACPD readings appear accurate to within ±1 mm for the full range of crack depth encountered in this test. Both seawater tests (SYNTHETIC#1 and NATURAL#2) display crack profiles having aspect ratios significantly higher than those for the air test. The narrower crack fronts observed for the seawater specimens are probably the consequence of an aggressive environment coalescing fewer initiation sites at a faster rate. The cracks which developed in seawater grew slightly off-center and never reached both sides of the specimen before rapid failure took place.

5.3.4 Behavior of Environmental Parameters

The environmental parameter which demonstrated the greatest variation among tests was current density. Although initial current densities were similar for all four specimens, the current decay transients were not (Figure 15, p.47). The current densities for

NATURAL#1 and SYNTHETIC#1 behaved erratically. This is thought to be a consequence of the stirring action created by the impellers of the miniature bilge pumps used initially with these specimens to pump the seawater back into the holding tanks. The current densities for the longer lasting specimens appear to stabilize after about 400,000 cycles. It is interesting to note that NATURAL#1 and NATURAL#2, which produced the shortest crack initiation periods, achieved the highest current densities during the early stages of testing. Note also that SYNTHETIC#1, which generated the fastest crack growth rates, assumed a long-term, steady-state current density about 2.5 times higher than that exhibited by NATURAL#2 or SYNTHETIC#2 (recall that the crack growth rates for NATURAL#2 were similar to those for the air test and that SYNTHETIC#2 failed to grow a crack).

Other environmental variables did not deviate significantly from their starting values. The pH readings for both seawater solutions rose slightly from 8.2 to about 8.4 during the first few days of testing and thereafter remained stable. Dissolved oxygen concentrations were effectively maintained near the saturation level (10 mg/liter for seawater at 5°C). Temperature fluctuations were less than ±1.5°C and the reference potential deviated by no more than ±5 mV in any one test.

6.0 DISCUSSION - *The Influence of Calcareous Deposits on Current Density and Fatigue Behavior*

It has been shown that the calcareous deposits which form within crevices can have a significant effect on the current density for water reduction. It has also been shown that the morphology and chemistry of these deposits can vary with bulk solution chemistry. Although the fatigue crack growth rates determined using CT specimens were not sensitive to the different seawaters, fatigue crack growth behavior in the welded T-plate specimens varied considerably between the two solutions. The purpose of the following discussion is to draw connections between deposit chemistry, current density, fatigue crack initiation and fatigue crack propagation, based on the results of this study. Table 6 (p.34) summarizes the results obtained from tests conducted at a temperature of 5°C and an electrochemical potential of -830 mV (SCE).

Calcareous deposits which precipitated within an artificial crevice polarized to -830 mV (SCE) in natural seawater reduced the current density for water reduction to a level almost 3 times below that achieved by deposits which formed under similar conditions in synthetic seawater. SEM analyses indicated that the deposits which formed from natural seawater were thin, but extremely rich in calcium. On the other hand, deposits which precipitated out of synthetic seawater were considerably thicker and contained primarily magnesium. Thus, the thin calcium rich deposits which formed in natural seawater were more effective at reducing the rate for water reduction than were the thicker magnesium rich deposits which formed in synthetic seawater under the same conditions of temperature and potential. For the welded T-plate specimens, these same conditions of temperature and potential produced crack growth rates that were about 2 times higher for synthetic seawater than for natural seawater.

Crack initiation for the T-plate specimens, however, took significantly longer in synthetic seawater than in natural seawater. Both specimens tested in natural seawater initiated 0.5 mm cracks more quickly than did the specimen tested in air. The current densities for NATURAL#1 and NATURAL#2 remained relatively high and fluctuated considerably throughout their initiation periods (Figure 15, p.47). These high, unstable current densities are an indication that calcareous deposits did not readily form on the exposed surfaces of NATURAL#1 and NATURAL#2. Crack initiation for SYNTHETIC#1 was delayed 100,000 cycles beyond the initiation point for the air test and

SYNTHETIC#2 failed to initiate a crack greater than 0.3 mm in depth. The current decay transients for SYNTHETIC#1 and SYNTHETIC#2 are indicative of cathodic steel surfaces that are quick to precipitate calcareous films. The current densities for both plates tested in synthetic seawater showed an early decline towards lower values. The current density for SYNTHETIC#2 dropped quickly and stabilized after about 300,000 cycles whereas that for SYNTHETIC#1 did not drop as fast and is seen to have risen after a cycle count corresponding closely to its crack initiation period. These facts would imply that the calcareous deposits which precipitated on SYNTHETIC#2 were more adherent and probably of greater thicknesses than the deposits which formed on SYNTHETIC#1. The ability of synthetic seawater to precipitate denser deposits than natural seawater within restricted crevices under the same experimental conditions used on the T-plates is also evident from an examination of Figures 6 and 7 (p.39).

Bell [27] has used finite element analysis to calculate the stress intensity factors for weld toe cracks in welded T-plates. For a T-plate loaded in 3-point bending, with a 45 degree weld profile and a crack 0.5 mm deep having an aspect ratio between 1.0 and 2.0, ΔK is estimated to be between 9 and 10 $MPa \cdot m^{1/2}$ for a weld toe stress range of 150 MPa. Vosikovsky [8] has shown that, under conditions which favour the precipitation of thick calcareous deposits, apparent threshold stress intensity ranges of 15 $MPa \cdot m^{1/2}$ for a stress ratio of 0.05 and of 10 $MPa \cdot m^{1/2}$ for a stress ratio of 0.5 may occur due to wedging effects. Although the T-plates tested in the present study utilized a load ratio of 0.05, the existence of residual tensile stresses in the weld toe region normally induce stress ratios that are closer to 0.5. Thus, if calcareous deposits are able to plug a crack before it can reach a critical depth (say 0.5 mm for a 150 MPa weld toe stress range), crack growth retardation or even crack arrest is possible. Furthermore, if apparent threshold stress intensity ranges as high as 10 $MPa \cdot m^{1/2}$ were possible for the T-plates tested in synthetic seawater, it would explain why initiation was delayed for SYNTHETIC#1 and why it failed to occur for SYNTHETIC#2. It can be seen from Table 6 (p.34) that, compared to air, the overall fatigue lives were longest for the T-plates tested in synthetic seawater. Undoubtably, this was due to the ability of synthetic seawater to delay crack initiation.

The fact that crack growth rates for the CT specimens tested in the two seawaters were not significantly different is probably a reflection of the short test duration (200,000 cycles or less). The absence of calcareous deposits within any of the CT specimens tested

at 5°C lends support to this assumption. The CT specimens were pre-cracked to a 15 mm depth in air and lasted for no more than two weeks from start to finish. Calcium rich nodules may not have had sufficient time to nucleate on the fracture surfaces the CT specimens tested in natural seawater. The T-plate experiments, on the other hand, began with a very slow initiation phase and generally lasted for six to eight weeks.

Both types of seawater were chemically analyzed in an attempt to uncover the reason behind the observed differences in calcareous deposits. Atomic absorption was used to determine the concentrations of calcium and magnesium ions in each of the two solutions. Salinities were measured using a refractometer. The results of these tests are summarized in Table 5 (p.34). The solutions were also analyzed for particulate matter using a Coulter counter (Figures 16 and 17, p.48). Inspection of Table 6 (p.34) would make it apparent that both solutions have similar major ion concentrations. Thus, the higher Ca:Mg ratios observed for calcareous deposits which formed from natural seawater were not simply the result of a higher concentration of calcium ions in solution. However, it is apparent from Figure 16 that natural seawater contains a greater number of particles in the 2-3 micron diameter range. If particles of this size play an important role in the nucleation and/or growth of calcium carbonate crystals, which are seen to be about 50 microns in diameter (Figure 7, p.39), it might explain why calcium rich deposits formed more readily within crevices exposed to natural seawater.

7.0 CONCLUSIONS

The results of this study would make it apparent that subtle differences in bulk solution chemistry can have a significant influence on the initiation and propagation of weld toe cracks under cathodic protection in 5°C seawater. The thick, magnesium rich deposits which form in synthetic seawater appear effective in delaying the initiation of short cracks, but act to enhance crack propagation once initiation has occurred. The thinner, calcium rich deposits which precipitate in natural seawater do not seem to affect crack initiation, but have been seen to promote slower crack propagation rates. The ability of calcareous deposits to delay initiation is thought to depend on their precipitation kinetics during the early stages of the test. If the rate of deposition is fast enough to plug the crack before it can reach a critical depth, crack growth retardation might be possible. The ability of calcareous deposits to influence crack propagation is thought to depend on their effectiveness in reducing the rate for water reduction on the fracture surface near the crack tip. Magnesium rich deposits appear to have little effect on the water reduction kinetics within crevices whereas it is possible for calcium rich deposits to reduce the rate for water reduction by an order of magnitude.

8.0 SUMMARY

The mechanical fatigue of welded tubular joints and the accelerated growth of cracks by seawater environments are critical issues concerning the integrity of steel structures used for offshore petroleum drilling and production. For fatigue cracks propagating under free corrosion, anodic dissolution is thought to be the predominant factor accelerating crack growth. When cathodic protection is used to suppress metal wastage, hydrogen charging of the highly stressed plastic zone in front of the crack tip can accelerate crack growth. The extent to which crack growth is enhanced by cathodic polarization is thought to depend on the properties of the mineral deposits that precipitate on the fracture surfaces near the crack tip.

Fatigue crack growth rates in the CT specimens tested in this study did not deviate significantly between natural and synthetic seawater solutions. In most cases, crack propagation rates were between 2 and 2.5 times faster under cathodic protection in seawater than in air. The welded T-plate specimens demonstrated a strong dependance on bulk solution chemistry. Fatigue cracks initiated early within the specimens tested in natural seawater, but propagated at rates close to those observed in air. Synthetic seawater prolonged the initiation phase but gave rise to crack propagation rates that were about 2 times higher than those observed in air.

It is not surprising that a wide scatter in test results has been found for fatigue crack growth rates measured under the influence of cathodic protection. It is apparent from this study that minor differences in seawater chemistry can have a significant effect on the chemistry and properties of the mineral deposits that form within a crack. The greater solubility and lower specific resistance of a magnesium rich deposit renders it less protective against water reduction than an insoluble calcium rich deposit. Thick, magnesium rich deposits appear to be beneficial in reducing the 'effective' ΔK (crack tip stress intensity range) but provide less resistance to reactant diffusion. The rate for water reduction on a surface coated with a magnesium rich deposit remains relatively high and this is thought to generate greater hydrogen embrittlement damage near the crack tip and a faster crack growth rate.

There is an obvious need for more information characterizing the composition and properties of deposits that form within fatigue cracks and the role these might play in influencing crack propagation rates. Many of the relationships suggested here are based on the results of a few tests carried out under specific conditions of stress, temperature and potential. Their validity should be checked against a wider range of conditions.

Table 1. Chemical analysis and mechanical properties of G40.21 Grade 350 WT steel.

ALLOYING ELEMENTS		MECHANICAL PROPERTIES	
C	0.22 max	MINIMUM YIELD STRESS	TENSILE STRENGTH
Mn	0.80/1.50	350 MPa	480/650 MPa
P	0.03 max		
S	0.04 max	MINIMUM ELONGATION	APPROXIMATE BRINELL HARDNESS
Si	0.15/0.40	19 %	140/190
other	0.10 max		

Table 2. Water reduction data obtained from artificial crevice experiments.

SURFACE GEOMETRY	ENVIRONMENT TYPE	TEMP (°C)	TEST POTENTIAL (mV vs. SCE)	TAFEL SLOPE (mV/decade)	CURRENT DENSITY * (uA/cm^2)
CREVICE	SYNTHETIC	5	-830	165	0.34
CREVICE	NATURAL	5	-830	115	0.12
CREVICE	SYNTHETIC	5	NO DEPOSITS	225	1.8
CREVICE	NATURAL	5	NO DEPOSITS	215	2.3
EXTERNAL	SYNTHETIC	5	NO DEPOSITS	150	2.4
EXTERNAL	NATURAL	5	NO DEPOSITS	200	6.4

* Current density is for the water reduction reaction @ -830 mV vs. SCE. Values were determined by extrapolation of the Tafel slope.

Table 3. Comparison of calcareous deposits found within artificial crevices polarized to -830 mV (SCE) at 5°C.

SEAWATER ENVIRONMENT	SAMPLE LOCATION	WEIGHT %				Ca:Mg
		Ca	Mg	Fe	Other	
SYNTHETIC	MOUTH/TOP	0.00	41.54	52.18	6.28	0.00
	MOUTH/BOTTOM	0.01	46.89	45.96	7.14	0.00
NATURAL	MOUTH/TOP	0.14	5.29	89.68	4.89	0.03
	MOUTH/BOTTOM	0.89	4.66	88.68	5.77	0.19
SYNTHETIC	CENTER/TOP	0.50	66.10	22.77	10.63	0.01
	CENTER/BOTTOM	0.49	63.82	23.58	12.11	0.01
NATURAL	CENTER/TOP	3.52	9.31	78.30	8.87	0.38
	CENTER/BOTTOM	2.57	8.76	78.72	9.95	0.29
SYNTHETIC	TIP/TOP	0.06	68.29	18.30	13.35	0.00
	TIP/BOTTOM	0.52	85.33	3.40	10.75	0.01
NATURAL	TIP/TOP	19.10	6.64	65.90	8.36	2.88
	TIP/BOTTOM	17.24	6.65	67.66	8.45	2.59

Table 4. Linear regression analysis of CT data.

TEST CONDITIONS	$da/dN = C(\Delta K)^m$	
	C	m
AIR @ 5°C	6.05×10^{-12}	3.03
SYNTHETIC SEAWATER @ 5°C	1.47×10^{-13}	4.55
NATURAL SEAWATER @ 5°C	1.94×10^{-12}	3.63

Table 5. Chemical analysis of seawaters.

	CONCENTRATION (ug/ml)		SALINITY (‰)
	Ca	Mg	
SYNTHETIC SEAWATER	40.0	133.6	37
NATURAL SEAWATER	38.6	123.3	34

Table 6. Overall Analysis of results for tests conducted at 5°C and -830 mV(SCE).

* refer to Table 2		SYNTHETIC SEAWATER	NATURAL SEAWATER
current density with deposit / current density without deposit		0.20 *	0.05 *
Ca : Mg (crevice tip)		0.01	2.88
crack growth rate in seawater / crack growth rate in air	T-plates	2.0-3.0	1.0-1.5
	CT's	~ 2.5	~ 2.0
crack initiation in seawater / crack initiation in air	T-plate#1	1.3	0.3
	T-plate#2	>3.3	0.5
fatigue life in seawater / fatigue life in air	T-plate#1	0.7	0.4
	T-plate#2	>1.1	1.0

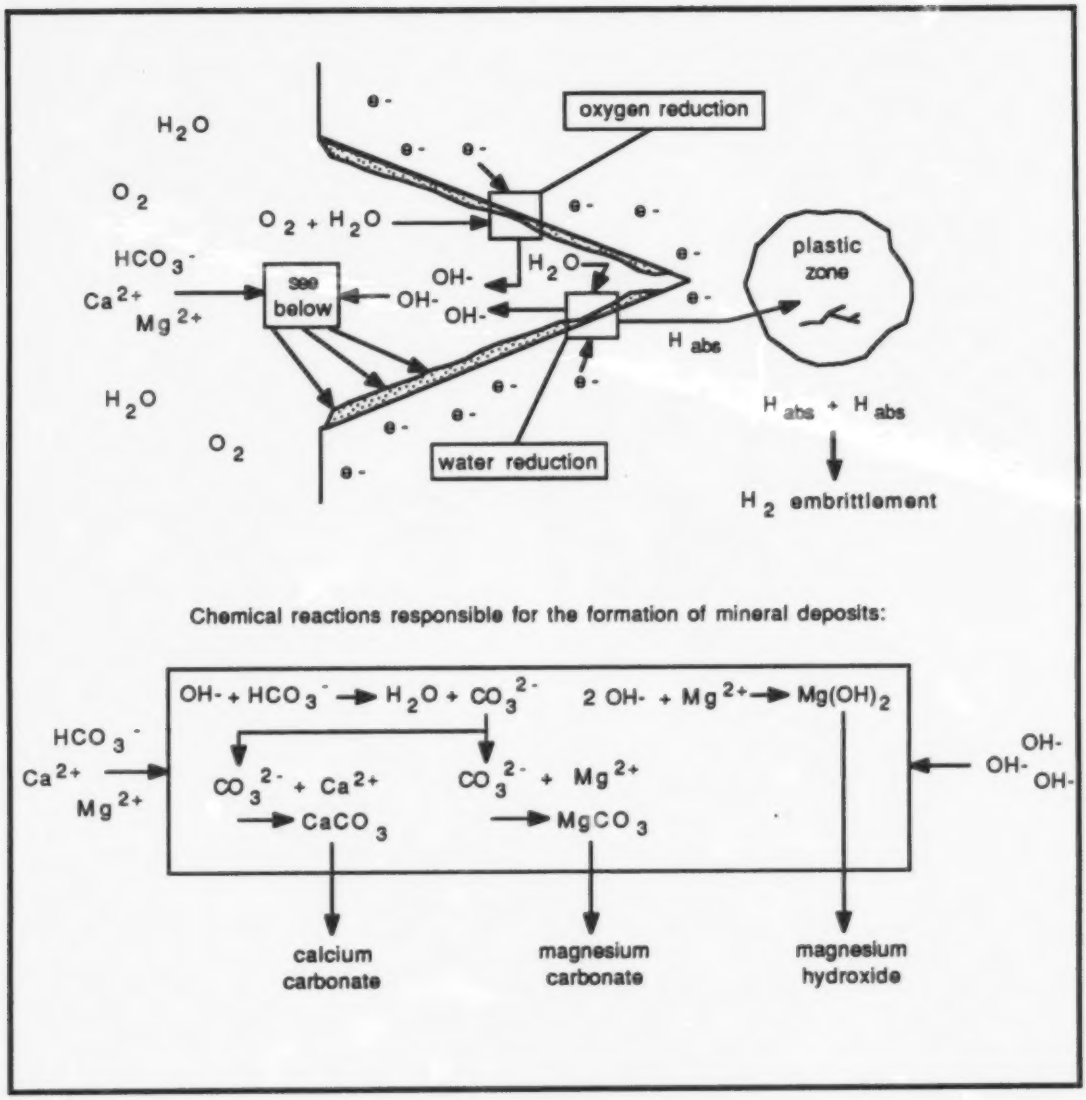

Figure 1. Simplified illustration of the electrochemistry within a fatigue crack under cathodic protection in seawater.

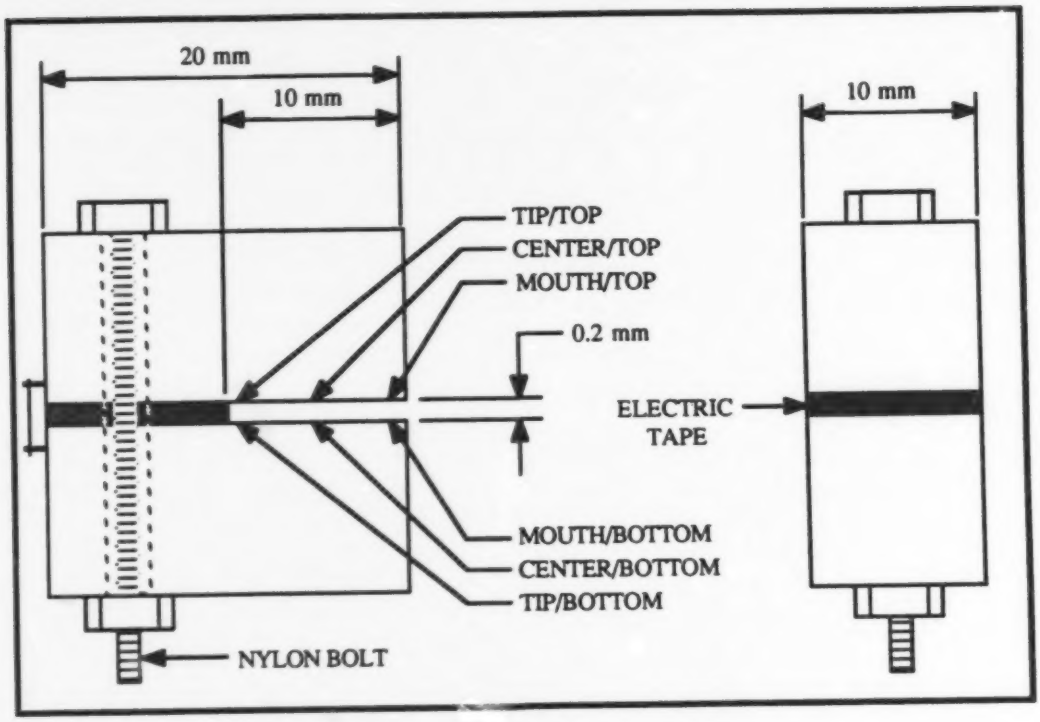

Figure 2. Artificial crevice assembly.

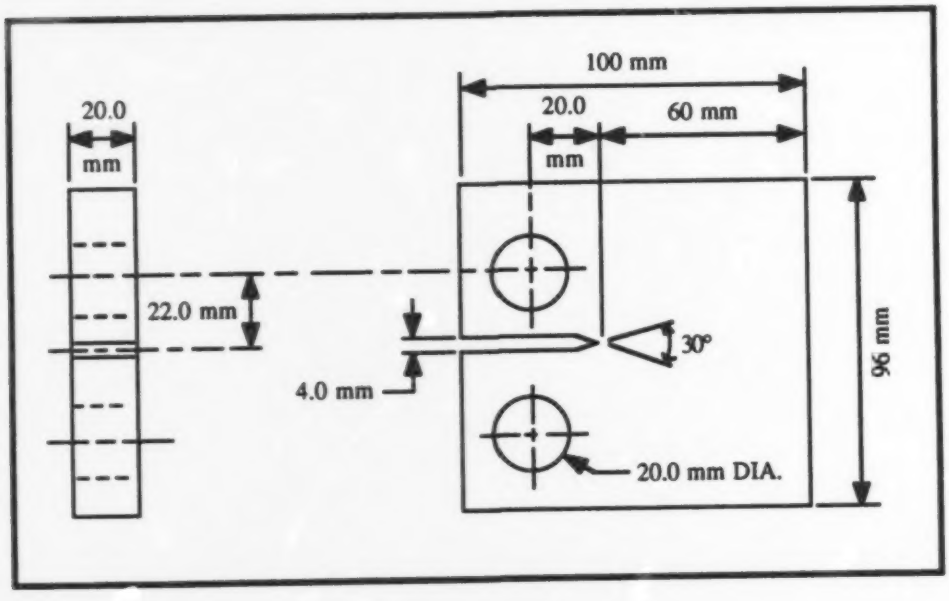

Figure 3. Compact type (CT) specimen geometry.

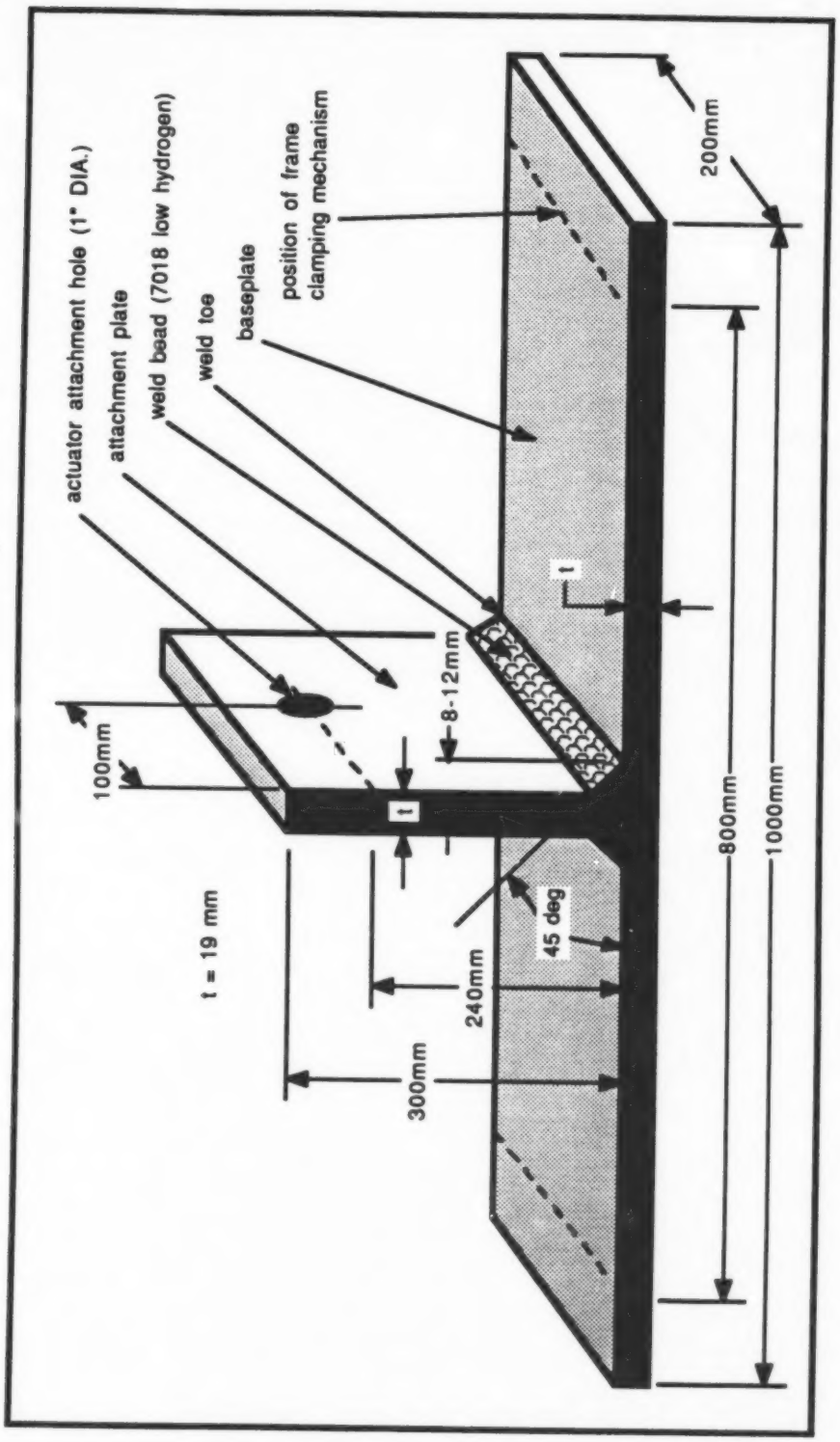

Figure 4. Welded T-plate geometry.

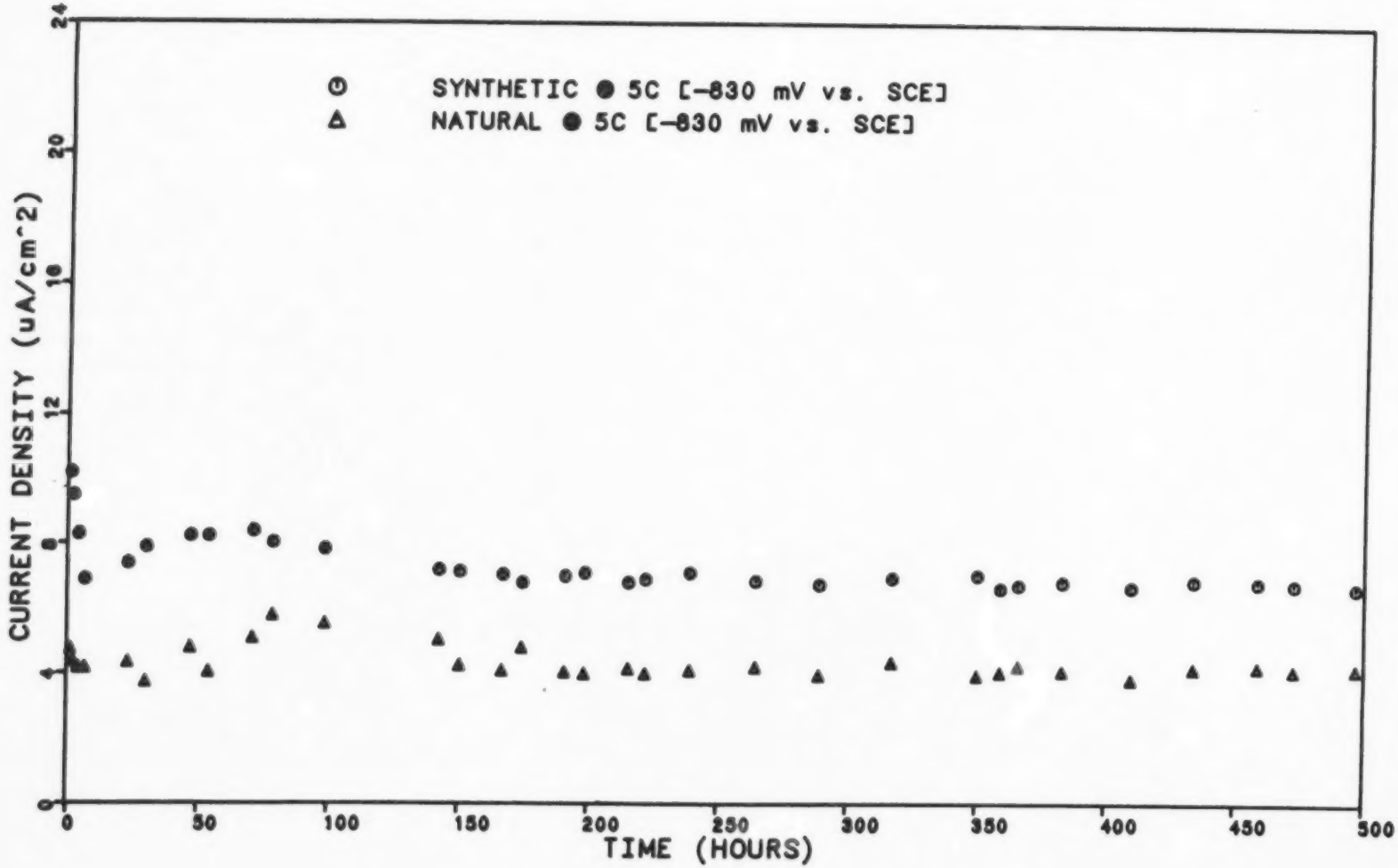

Figure 5. Current decay transients for artificial crevices polarized to -830 mV (SCE) @ 5°C.

ELEMENT	Ca	Mg	Fe	other
WT%	0.52	85.33	3.40	10.75

Figure 6. SEM analysis of calcareous deposits near tip of artificial crevice polarized to -830 mV (SCE) in 5°C synthetic seawater.

ELEMENT	Ca	Mg	Fe	other
WT%	19.1	6.64	65.9	8.36

Figure 7. SEM analysis of calcareous deposits near tip of artificial crevice polarized to -830 mV (SCE) in 5°C natural seawater.

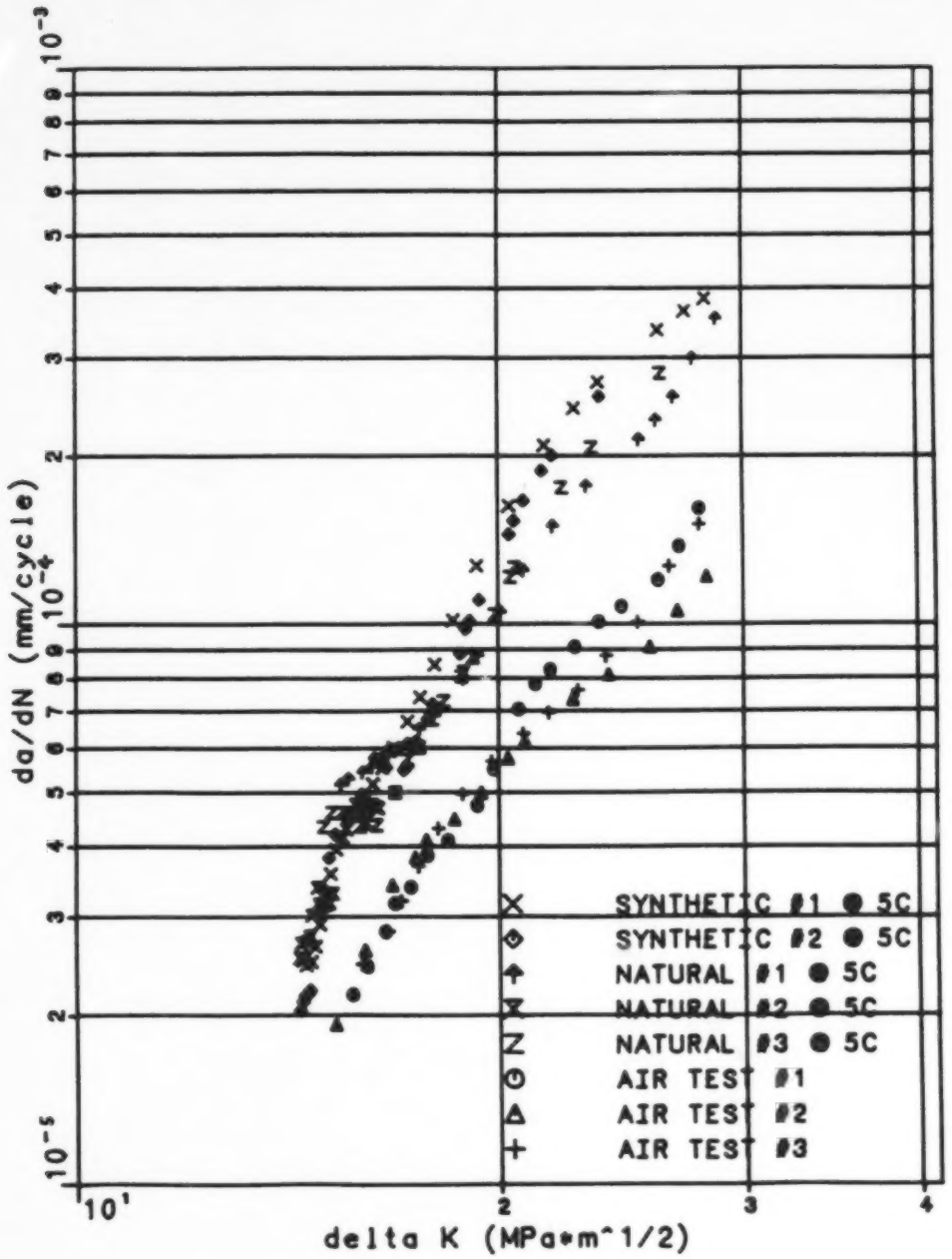

Figure 8. Comparison of fatigue crack propagation data for CT specimens tested in air with CT specimens tested at -830 mV (SCE) in natural and synthetic seawaters at 5°C.

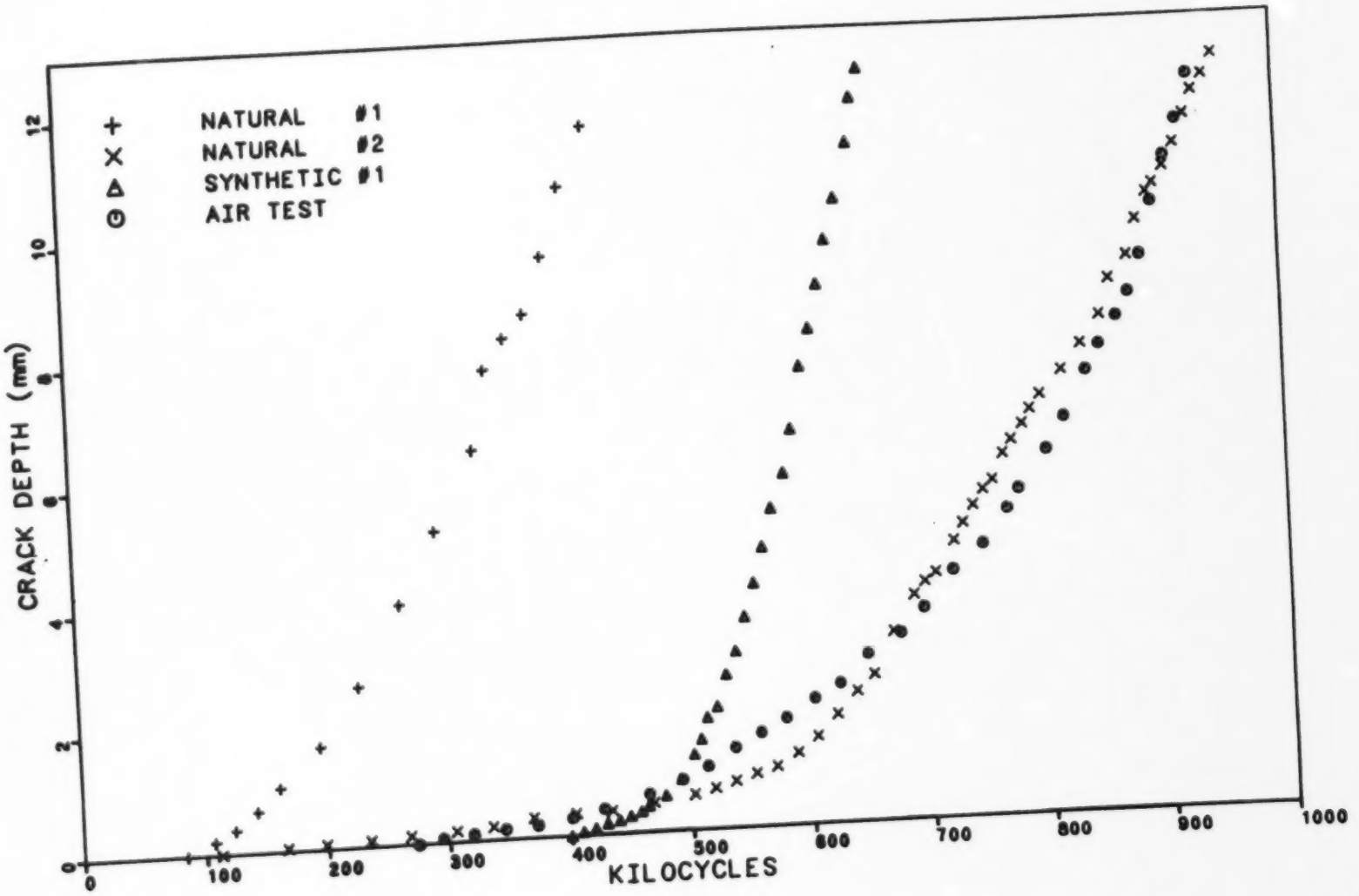

Figure 9. Crack depth as a function of elapsed cycles for the welded T-plate specimens.

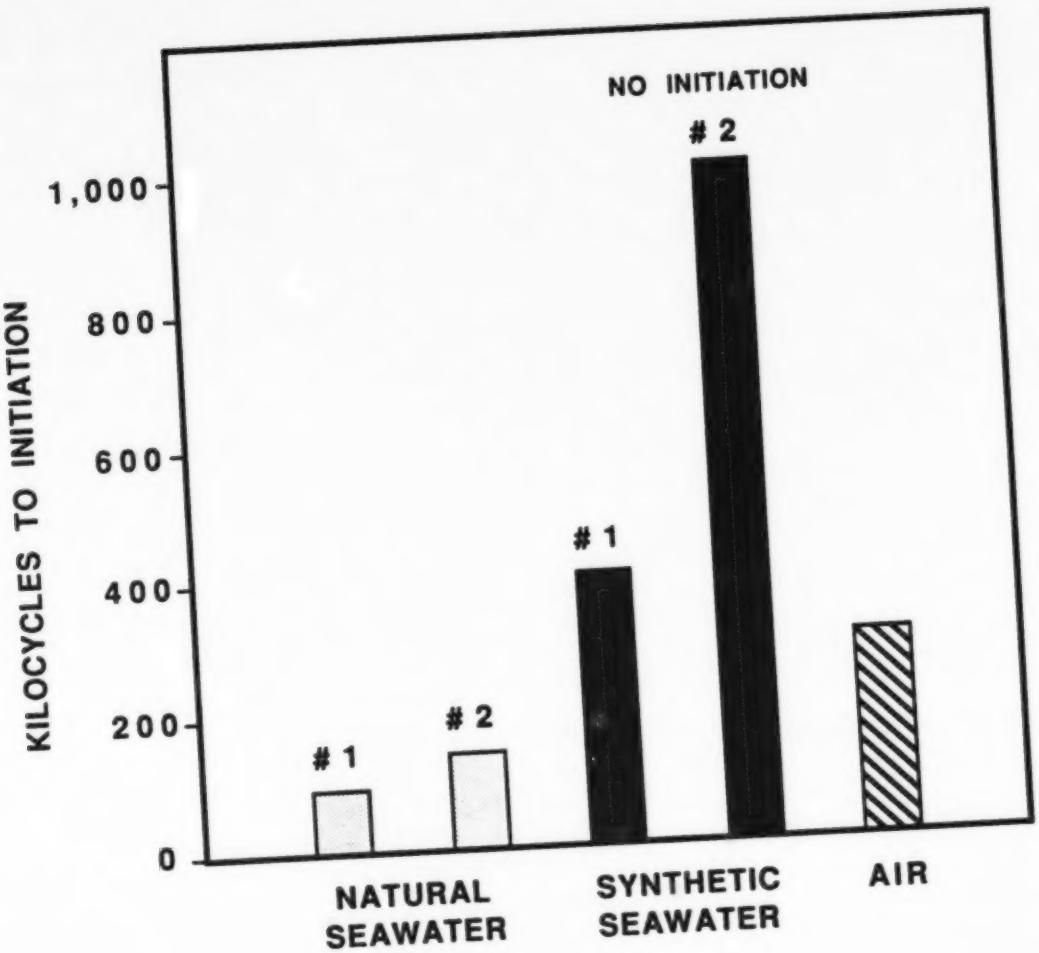

Figure 10. Comparison of cycles to initiation for the welded T-plate specimens.

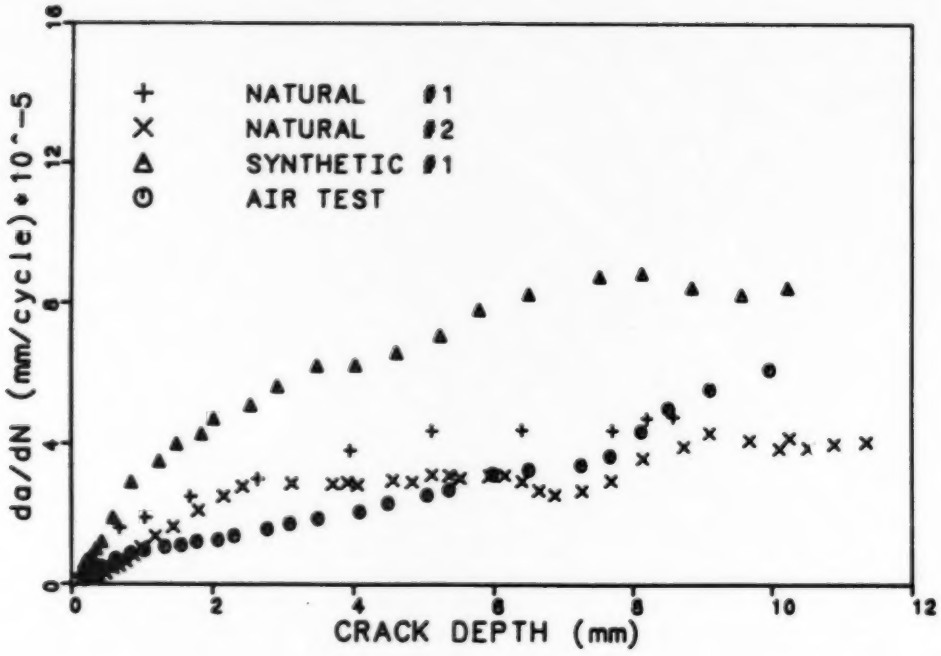

Figure 11. Fatigue crack propagation rate as a function of crack depth for the welded T-plate specimens.

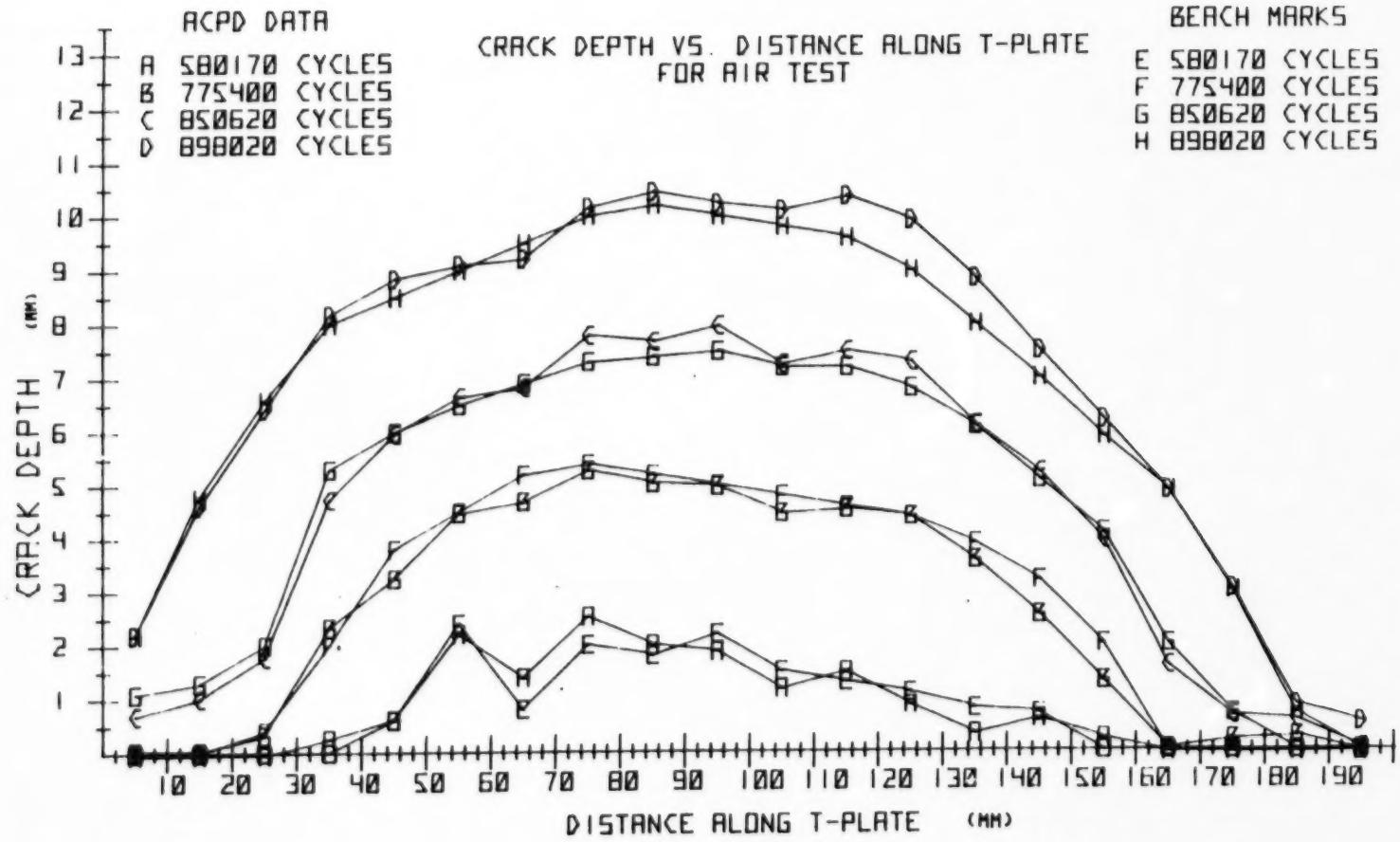

Figure 12. Comparison of ACPD readings with beach marks for the welded T-plate specimen tested in air.

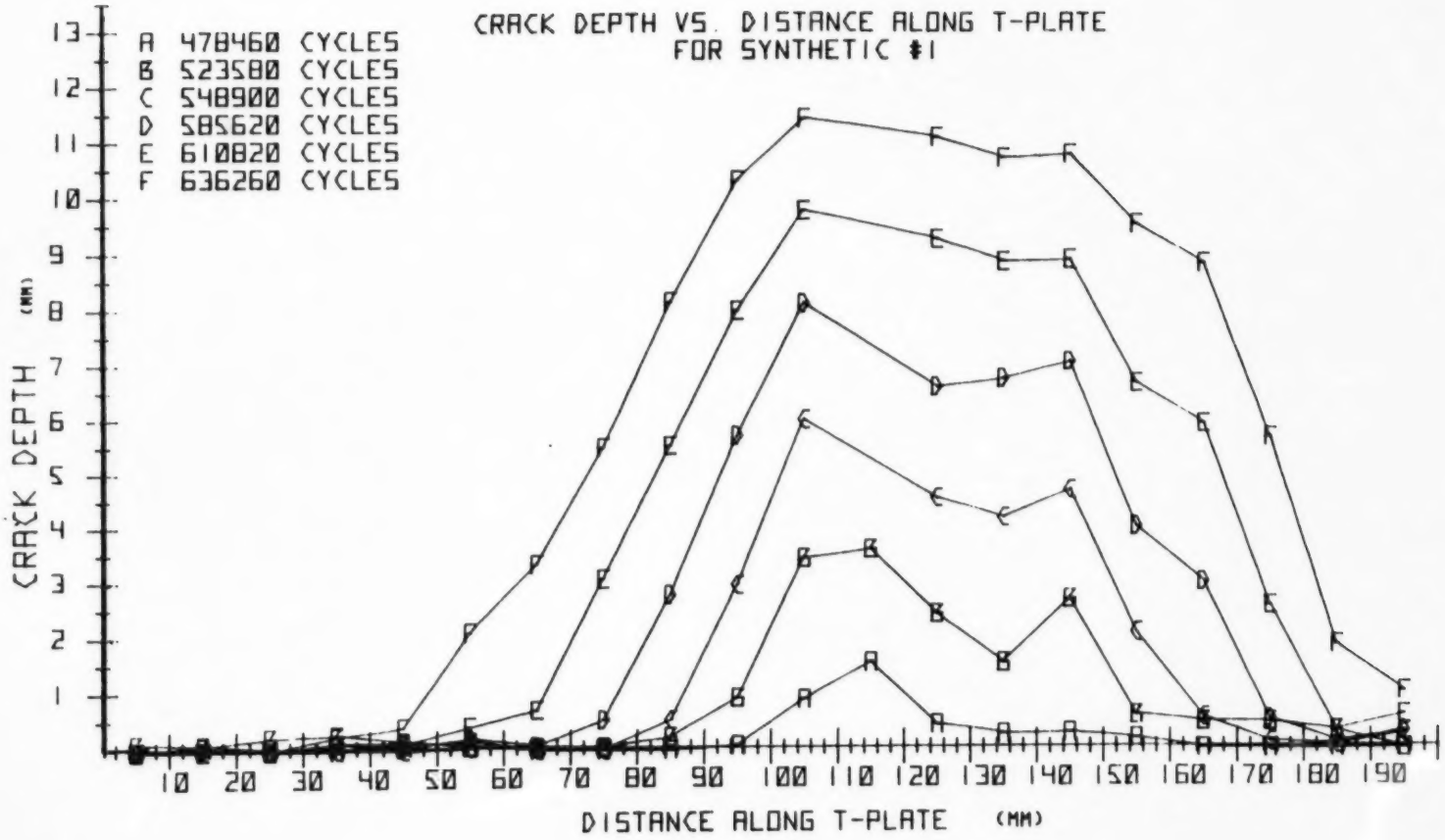
CRACK DEPTH VS. DISTANCE ALONG T-PLATE
FOR SYNTHETIC #1
A 478460 CYCLES
B 523580 CYCLES
C 548900 CYCLES
D 585620 CYCLES
E 610820 CYCLES
F 636260 CYCLES
CRACK DEPTH (MM)
DISTANCE ALONG T-PLATE (MM)
1 2 3 4 5 6 7 8 9 10 11 12 13
10 20 30 40 50 60 70 80 90 100 110 120 130 140 150 160 170 180 190

Figure 13. Crack profiles for a welded T-plate specimen tested in 5°C synthetic seawater.

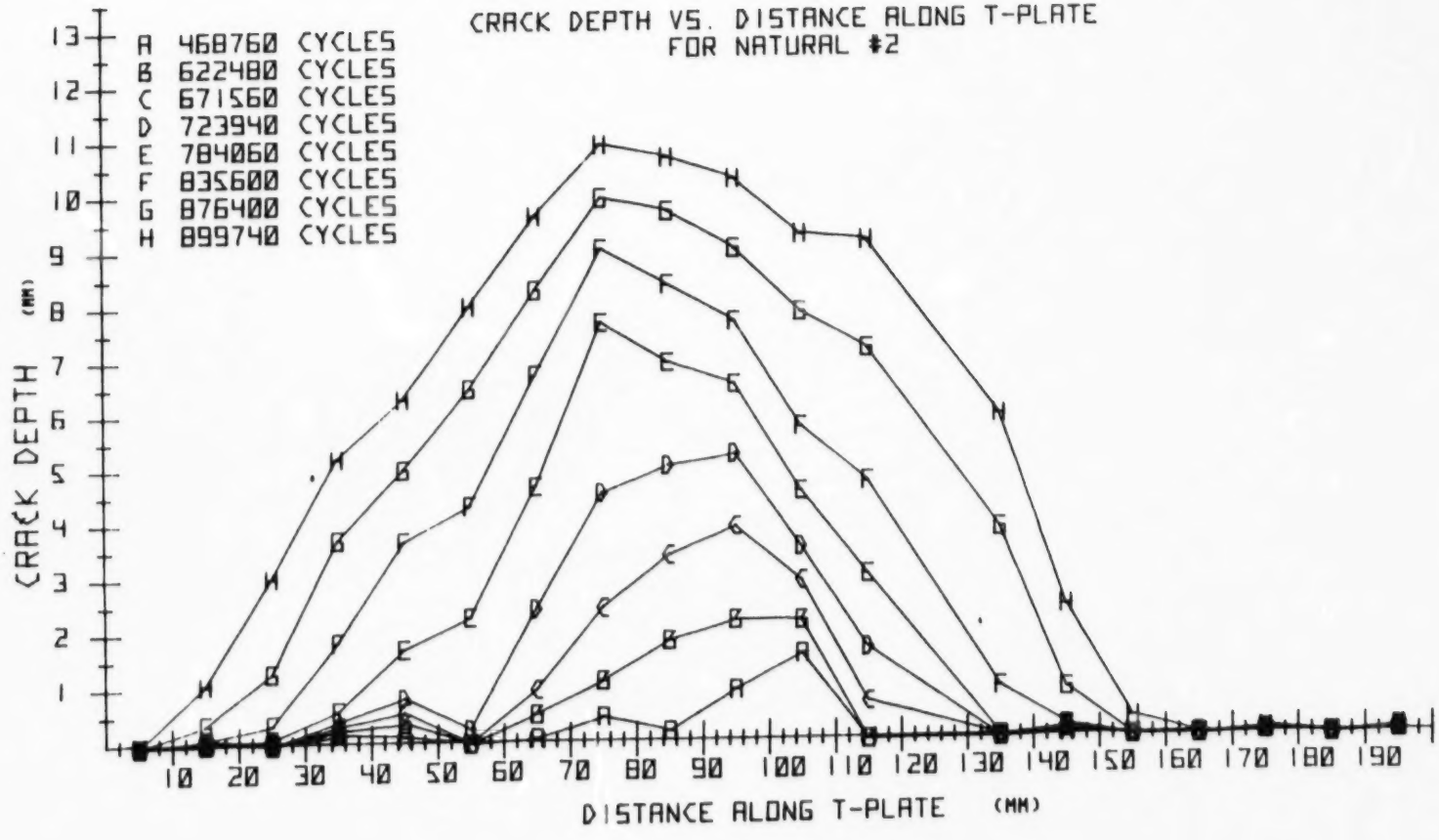

Figure 14. Crack profiles for a welded T-plate specimen tested in 5°C natural seawater.

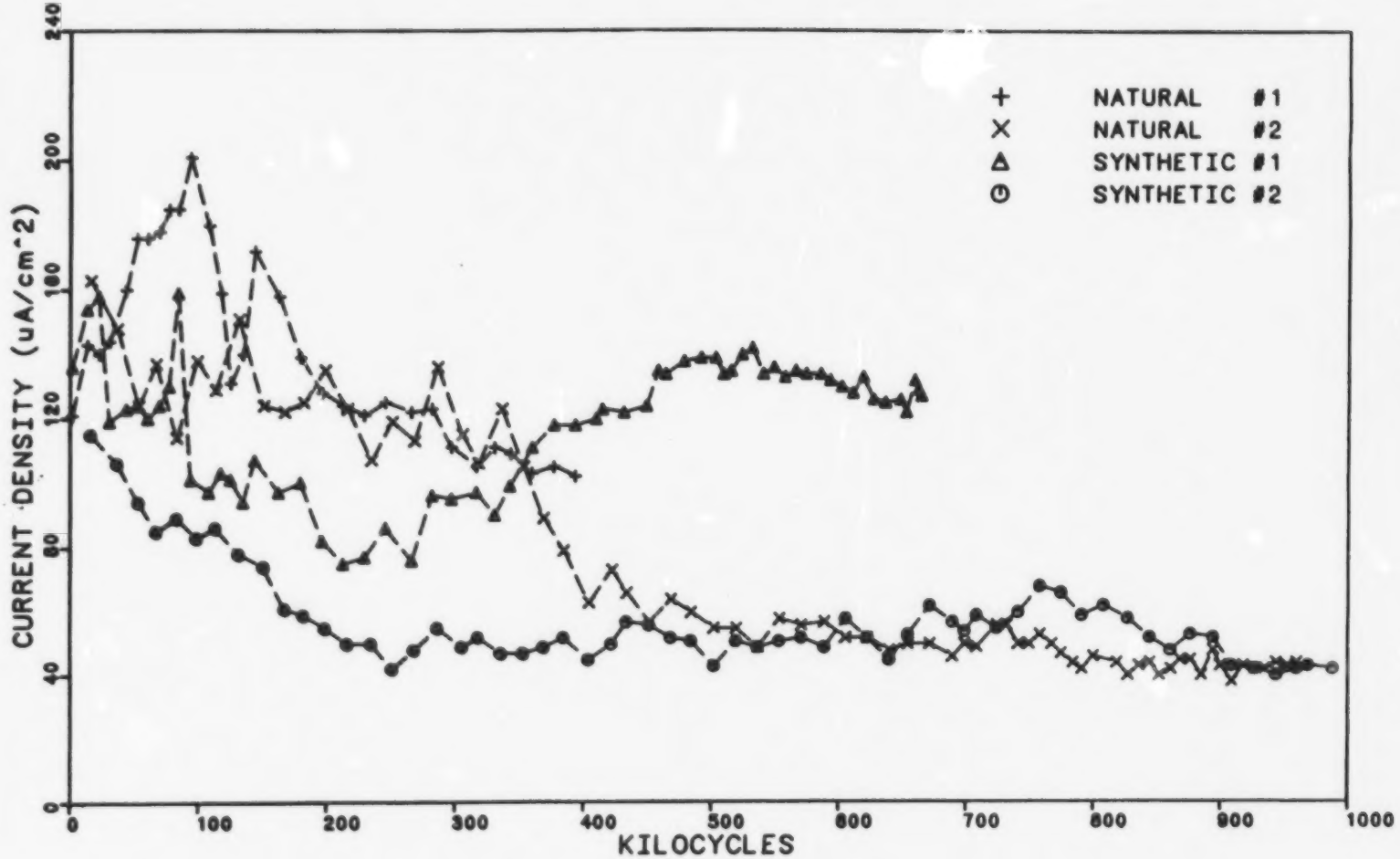

Figure 15. Current decay transients for welded T-plate specimens tested in 5°C seawater.

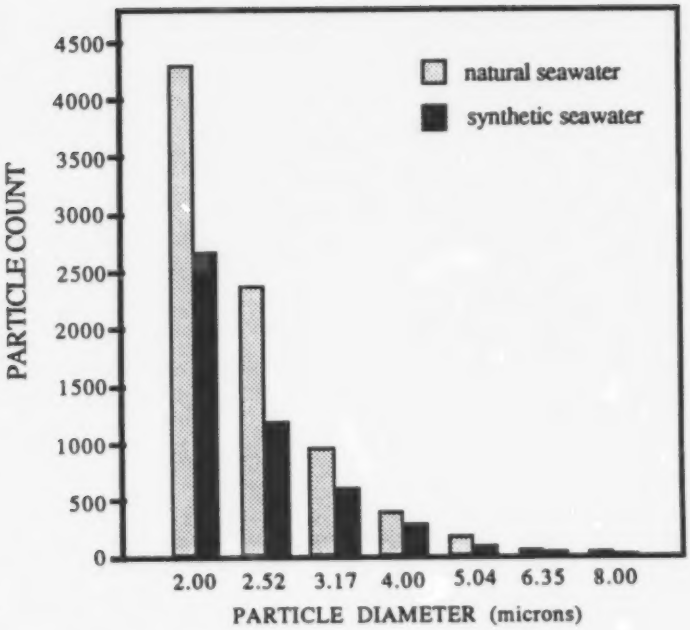

Figure 16. Distribution of particle size in 2 ml of solution for a 100 micron diameter aperture.

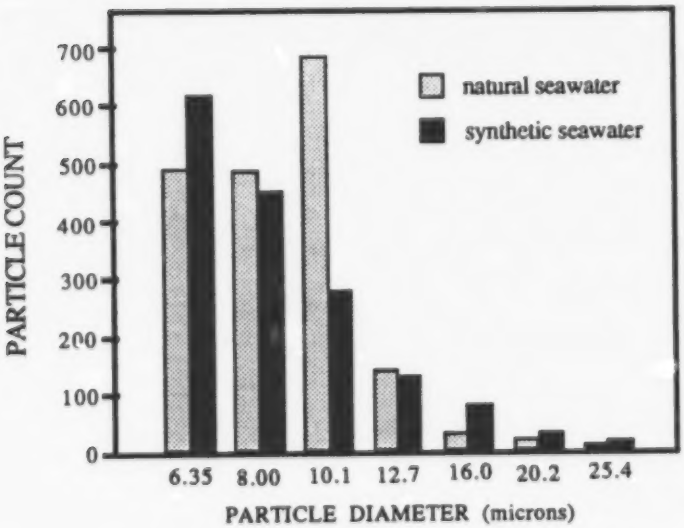

Figure 17. Distribution of particle size in 2 ml of solution for a 280 micron diameter aperture.

REFERENCES

1. P.M. Scott, "Chemistry Effects in Corrosion Fatigue", Corrosion Fatigue: Mechanics, Metallurgy, Electrochemistry, and Engineering, ASTM STP 801, T.W. Crooker and B.N. Leis, Eds., American Society for Testing and Materials, p.319 (1983)

2. E.G. Daft, K. Bohenkamp, H.J. Engell, "Investigations of the Hydrogen Evolution Kinetics and Hydrogen Absorption by Iron Electrodes During Cathodic Polarization", Corrosion Science, Vol. 19, No. 9, p.591 (1979)

3. B.S. Chaudhari, T.P. Radhakrishnan, "The Uptake of Cathodic Hydrogen by Shim Steel", Corrosion Science, Vol. 25, No. 11, p.1077 (1985)

4. C.G. Interrante, "Proceedings First International Conference on Current Solutions to Hydrogen in Steels", C.G. Interrante, G.M. Pressouyre, Eds., ASM Metals Park, Ohio, p.3 (1982); Ref.3, p.1077

5. H.C. Rogers, "Hydrogen Embrittlement in Engineering Materials", Corrosion Source Book, S.K. Coburn, Ed., American Society for Metals, p.312 (1984)

6. P.M. Scott, "The Effects of Sea Water on Corrosion Fatigue in Structural Steels", Corrosion Fatigue, R.N. Parkins, Ya.M. Kolotyrkin, Eds., Proceedings of the First USSR-UK Seminar on Corrosion Fatigue of Metals held in Lvov, USSR, 19-22 May 1980, published by The Metals Society, p.89 (1983)

7. O. Vosikovsky, "Fatigue-Crack Growth in an X-65 Line-Pipe Steel at Low Cyclic Frequencies in Aqueous Environments", Transactions of the ASME, Journal of Engineering Materials and Technology, Series H, Vol. 97, No. 4, p.298 (1975)

8. O. Vosikovsky, W.R. Neill,D.A. Carlyle, A. Rivard, "The Effect of Seawater Temperature on Corrosion Fatigue Crack Growth in Structural Steels"; CANMET Report, Physical Metallurgy Research Laboratories (1983)

9. Zhi-Shen Tong, Ming-Qi Li, Bo-Xue Feng, Yue Shi, "The Corrosion Fatigue of SiCrMoCuV Steel in 3.5% NaCl Solution", Corrosion, Vol. 41, No. 3, p.121 (1985)

10. S.J. Hudak, Metall. Trans., Vol. 7A, No. 2, p.235 (1976); Ref.12, p.80

11. R.A. Cottis, D.C.A. Moore, "Hydrogen Uptake By Steel Under Marine Fouling Growths", Proceedings of the 9th International Congress on Metallic Corrosion, Toronto, p.538 (1984)

12. I.I. Vasilenko, V.I. Kapinos, The Role of Adsorption, Dissolution and Hydrogen Embrittlement Processes During the Fatigue Failure of Steels in Aggressive Environments", Corrosion Fatigue, R.N. Parkins, Ya.M. Kolotyrkin, Eds., Proceedings of the First USSR-UK Seminar on Corrosion Fatigue of Metals held in Lvov, USSR, 19-22 May 1980, published by The Metals Society, p.74 (1983)

13. P.M. Scott, T.W. Thorpe, D.R.V. Silvester, "Rate-Determining Processes for Corrosion Fatigue Crack Growth in Ferritic Steels in Seawater", Corrosion Science, Vol. 23, No. 6, p.559 (1983)

14. H. Arup, E. Maahn, F. Jacobsen, P. Press, "Environmental Effects in Corrosion Fatigue", ECSC Agreement Number 7210 KG. 901, Final Report, Work done at Korrosionscentralen, Danish Metallurgy Dept., Danish Technical University (1982-1983)

15. Ernst Maahn, "Crack Tip Chemistry Under Cathodic Protection and Its Influence on Fatigue Crack Growth",Work done at Korrosionscentralen, Danish Metallurgy Dept., Danish Technical University (1986)

16. William C. Hooper, William H. Hartt, "The Influence of Cathodic Polarization Upon Fatigue of Notched Structural Steel in Seawater", Corrosion, Vol. 34, No. 9, p.320 (1978)

17. E. Maahn et. al, "Environmental Effects in Fatigue Crack Initiation and Propogation", Technical Report No. 4 - Project No. 7210.KG/902, Work done at Korrosionscentralen, Danish Metallurgy Dept., Danish Technical University (1986)

18. S.L. Wolfson, W.H. Hartt, "An Initial Investigation of Calcareous Deposits Upon Cathodic Steel Surfaces in Seawater", Corrosion, Vol.37, No. 2, p.70 (1982)

19. A. Turnbull, D.H. Ferriss, "Mathematical Modelling of the Electrochemistry in Corrosion Fatigue Cracks in Structural Steel Cathodically Protected in Sea Water", Corrosion Science, Vol. 26, No. 8, p.601 (1986)

20. William H. Hartt, Charles H. Culberson, Samuel W. Smith, "Calcareous Deposits on Metal Surfaces in Seawater - A Critical Review", Corrosion, Vol. 40, No. 11, p.609 (1984)

21. Charles H. Culberson, "Effect of seawater Chemistry on the Formation of Calcareous Deposits", Paper #61 presented at NACE Conference "Corrosion '83", April 18-22 (1983)

22. J.R. Ambrose, A.E. Yaniv, U. Rupert Lee, "Nucleation, Growth and Morphology of Calcareous Deposits on Steel in Seawater", Paper #60 presented at NACE Conference "Corrosion '83", April 18-22 (1983)

23. M. Habashi, G. Philipponneau, S. Widawski, J. Galland, "Interactions Between Fatigue Crack Growth Rate and Kinetics of Magnesium Calcium Rich Deposits Formation at the Crack Tip of Mild Steel Cathodically Polarised in Sea Water", Proceedings ICF6, Conference, New Delhi, p.2521 (1984)

24. H.S. Preiser, B.L. Silverstein, Journal of Navigation Engineering, p.881 (1950); Ref.22, p.3

25. K.A. Lucas, M.J. Robinson, "The Influence of Lattice Hydrogen Content on the Hydrogen-Assisted Cracking of High Strength Steel", Corrosion Science, Vol. 26, No. 9, p.705 (1986)

26. A. Turnbull, M.K. Gardner, "Electrochemical Polarization Studies of BS 4360 50D Steel in 3.5% NaCl", Corrosion Science, Vol. 22, No. 7, p.661 (1982)

27. R. Bell, "Stress Intensity Factors For Weld Toe Cracks in Welded 'T' Plate Joints", CANMET Report, D.S.S. Contract OST84-00125, Faculty of Engineering, Carleton University, Ottawa (1987)

APPENDIX

◆ SYNTHETIC/CREVICE ● 5C (NO DEPOSITS)
✦ NATURAL/CREVICE ● 5C (NO DEPOSITS)
⊙ SYNTHETIC/EXTERNAL ● 5C (NO DEPOSITS)
▲ NATURAL/EXTERNAL ● 5C (NO DEPOSITS)

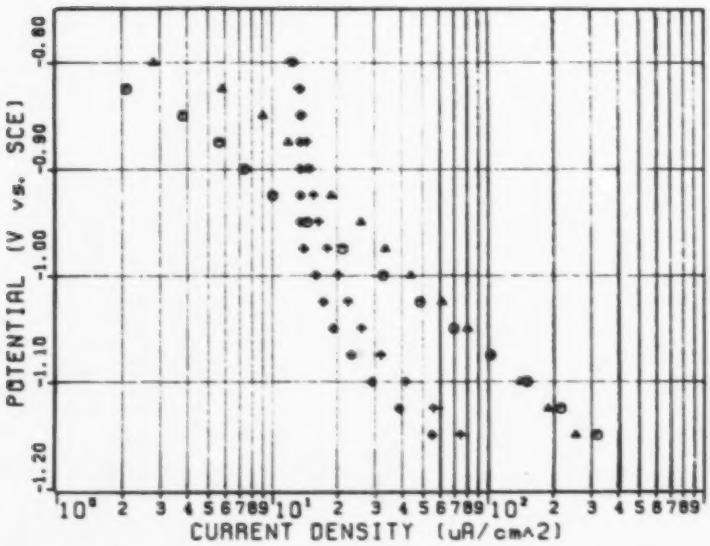

Y SYNTHETIC/CREVICE ● 5C (-830 mV SCE)
✖ NATURAL/CREVICE ● 5C (-830 mV SCE)
◆ SYNTHETIC/CREVICE ● 5C (NO DEPOSITS)
✦ NATURAL/CREVICE ● 5C (NO DEPOSITS)